Free vibration of FGM Mindlin plates submerged in fluid

Hui-Cui Li[a], Liao-Liang Ke[a,b1], Zhang-Ming Wu[c,d], Jie Yang[e]

[a] *Department of Mechanics, Beijing Jiaotong University, Beijing, 100044, China*

[b] *School of Mechanical Engineering, Tianjin University, Tianjin, 300350, China*

[c] *School of Mechanical Engineering and Mechanics, Ningbo University, Ningbo, 315211, China*

[d] *School of Engineering, Cardiff University, Cardiff CF24 3AA, UK*

[e] *School of Engineering, RMIT University, Bundoora, VIC 3083, Australia*

Abstract. This paper presents a free vibration analysis of functionally graded material (FGM) plates that are partially submerged in an incompressible, inviscid fluid. The FGM plates with four gradient types of continuously varying material properties along the thickness direction, including the power law, exponential, sinusoidal and cosine forms, are studied to examine various distributions of material properties. The plate is modeled based on the Mindlin Plate Theory (MPT), and the fluid loading effect on the FGM plates is modeled using the method of added mass. The variational principle is applied to derive the governing equations of this fluid-plate interaction system. The differential quadrature (DQ) method is used to solve this problem by converting the governing equations into a system of linear equations. The fundamental frequency and the corresponding mode shape are obtained using an iterative procedure. Numerical results for several examples are obtained and presented to investigate the vibration characteristics of the submerged FGM plates in terms of the gradient index, gradient type, immersed depth, fluid density, aspect ratio and slenderness ratio. Results indicate that the larger aspect ratio and immersed depth increase the fundamental frequency of the FGM plate, while larger gradient index, fluid density and slenderness ratio decrease the fundamental frequency. Among four different material gradient types, the FGM plate with power law type gradient has the smallest fundamental frequency, while the one with sinusoidal form has the largest value. The mode shape in fluid deviates from that in vacuum and shows an unsymmetrical shape for CCCC and SSSS FGM plates.

Keywords: FGM plates; Free vibration; Added mass method; Fluid-plate interaction

[1] Corresponding author. llke@bjtu.edu.cn (L. L. Ke)

1. Introduction

Functionally graded materials (FGM), which are one of the most advanced inhomogeneous composites and have attracted broad engineering applications, are characterized by their mixture of continuously varying distributions of components with different distinct properties. FGMs are usually made from the metals-ceramics mixture, of which the material properties are allowed to vary continuously, such as Poisson's ratio, mass density and elastic modulus described by the power law distribution, exponential distribution, etc. [1,2]. FGMs take advantage of the different materials to maintain structural integrity, such as metals with strong mechanical performance, ceramics with high thermal resistance, and so on [3]. With the increasing maturity of advanced material manufacturing technology, the FGMs have been extensively applied in various industrial sectors, such as aerospace, automobile, biomedical engineering, and civil engineering [4,5].

Plate structures have received wide engineering applications in many fields, such as architecture, aviation, shipbuilding and so on. Several plate theories [6–8] have been developed by researchers to model the mechanical behaviors of plates under various loading cases and boundary conditions. The Kirchhoff plate theory [8,9] is introduced to model the mechanical behaviors of thin plates with an assumption that straight lines normal to the middle surface remain straight and normal to the deformed middle surface during deformation, and thus only considering the bending deformation and stretching deformation. This thin plate theory often overestimates the natural frequencies of the moderately thick plates because the shear deformation effect is not negligible for thick plates. Consequently, considering the shear deformation effect is necessary in the modelling and analysis of moderately thick plates. The plate theories considering the shear deformation effect, such as the Mindlin plate theory [10] and the Reddy plate theory [11], were proposed to establish relatively precise models for moderately thick plates.

Based on these plate theories, the mechanical behaviors, such as bending [12–14], vibration [15–18], buckling [19–22] and dynamic stability [23,24], of moderately thick plates have been well studied in many previous research works. For example, the vibration problems of FGM plates have been extensively investigated by many research works either theoretically or numerically [25–30]. An exact solution for the vibration of the rectangular FGM plates was derived by Hosseini-Hashemi *et al.* [31]. Kim *et al*. [32] presented a frequency analysis of FGM plates using the Ritz method and the ultraspherical polynomials as the shape functions. Wang and Shen [33] analyzed the vibration of FGM nanoplates with reinforced composites. Zhao *et al*. [34] performed the vibration analysis of FGM Mindlin plates using the kernel particle method and the Ritz method. These research works mentioned above only focused on the vibration behavior of FGM plate in vacuum, namely without any fluid loadings. Nevertheless, the study of FGM plates in fluids remains importance due to its broad engineering applications in shipbuilding, biomedical devices and

aerospace structures. Farsani *et al*. [35] analyzed the vibration behavior of functionally graded porous plates, only one side of which is contact with fluid, using the Ritz method. Thinh *et al*. [36] examined the vibration characteristics of a horizontal FGM rectangular plate in fluid using the Navier's approach.

Extensive analyses for the vibration of homogeneous plate structures in fluid environment have been carried out due to its wide applications in ocean engineering, biomedical engineering, and aerospace engineering. In these research works, different fluid properties including the compressible and incompressible fluid [37–40], viscid and inviscid fluid [41–44], are considered. Up to date, most studies on the plate-fluid coupling system mainly focused on the ideal fluid for the purpose of simplifying the theoretical analysis procedures. Canales and Mantari [45] presented the vibration analysis of Mindlin plates in fluid using the Ritz method and validated by 3D finite element method. The vibration of Kirchhoff plates contacted with water was studied by Zhou and Cheung [46]. Omiddezyani *et al*. [47] performed the vibration analysis of Mindlin microplates contacted with fluid. They studied both bulging modes and sloshing modes due to the existence of deformation effect and sloshing effect of fluid. Khorshidi *et al*. [48] theoretically and experimentally analyzed the vibration of a Kirchhoff plate in fluid using the Ritz method and the acoustic testing method, respectively. Using the digital laser vibrometer, Bochkarev *et al*. [49] experimentally measured the nature frequencies of rectangular plates vibrating in a fluid. Up to now, vibrations of FGM structures partially immersed in fluid have been rarely studied in the field of fluid-plate interaction. However, these analyses are necessary for the design of structures partially immersed in fluid, such as shipbuilding, sensors, bio-MEMS, etc.

This paper analyzes the free vibration of rectangular Mindlin FGM plates interacted with fluid. The gradient variation of the FGM plate along the thickness direction is considered, and different gradient types of FGM plates are discussed. The fluid effect is modeled as an added mass to the vibrating plates. The linear governing equations of discretized form are obtained using the DQ method. An iterative procedure is applied to obtain the numerical solutions for the fundamental frequency and the mode shape. The fluid-loading influences in terms of the gradient index, gradient type, fluid density, slenderness ratio and aspect ratio on the vibration characteristics of FGM plates are studied using the present modelling method and discussed.

2. Formulation

In Fig. 1, a rectangular FGM plate with thickness h_0, height L_x and width L_y is vertically and only partially immersed into a fluid with a depth L_1. Fig. 1 shows a schematic diagram for the spatial geometry of this plate and its xOz section immersed in a fluid within the Cartesian coordinate system $Oxyz$. The FGM plate is made of a metal-ceramic mixture with 100% of metal and 100% of ceramic on the left and right surfaces, respectively. The

variation of material properties is continuous and smooth along the z-axis with four gradient types, namely the power law, exponential, sinusoidal and cosine forms. The FGM plates mainly analyzed by the power law form and other forms are given for comparison in the discussion. The Young's modulus $E(z)$, Poisson's ratio $\nu(z)$ and mass density $\rho(z)$ of the power law form are computed as [50],

$$E(z) = (E_b - E_a)\left(\frac{1}{2} + \frac{z}{h_0}\right)^n + E_a, \tag{1}$$

$$\nu(z) = (\nu_b - \nu_a)\left(\frac{1}{2} + \frac{z}{h_0}\right)^n + \nu_a, \tag{2}$$

$$\rho(z) = (\rho_b - \rho_a)\left(\frac{1}{2} + \frac{z}{h_0}\right)^n + \rho_a, \tag{3}$$

where n is the gradient index; subscripts a and b refer to the physical quantity of metal at $z = -h_0/2$ and ceramic at $z = h_0/2$, respectively.

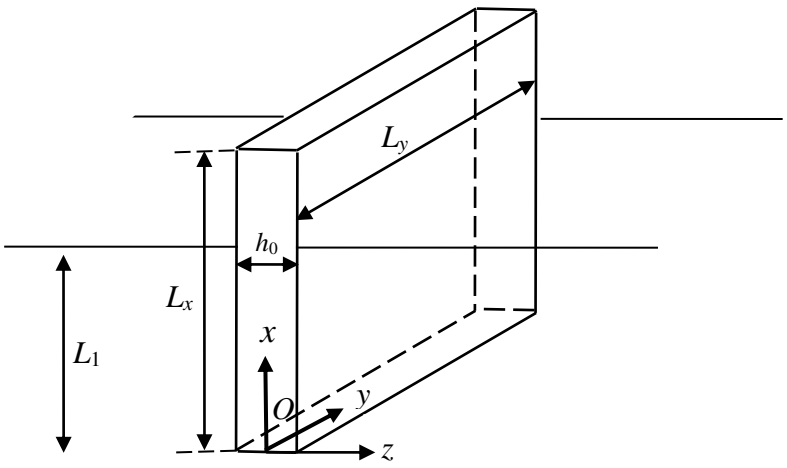

Fig. 1. An FGM plate Schematics in fluid.

2.1 Hydrodynamic pressure

In this fluid-plate coupling system, we assume an ideal fluid, which is irrotational, incompressible, and inviscid. Therefore, the damping effect and the sloshing effect of the fluid are ignored in this study. The velocity potential of fluid domain φ is satisfied the following Laplace's equation [46] as,

$$\nabla^2 \varphi = 0, \tag{4}$$

and the corresponding boundary conditions,

$$\frac{\partial \varphi}{\partial x}\Big|_{x=0} = 0, \ \varphi\Big|_{x=L_1} = 0, \tag{5a}$$

$$\left.\frac{\partial \varphi}{\partial y}\right|_{y=0}=0,\ \left.\frac{\partial \varphi}{\partial y}\right|_{y=L_y}=0, \tag{5b}$$

$$\left.\frac{\partial \varphi}{\partial z}\right|_{z=\pm\frac{h_0}{2}}=\frac{\partial W_1(x,y,t)}{\partial t}, \tag{5c}$$

$$\left.\varphi\right|_{z\to\pm\infty}=0, \tag{5d}$$

where $W_1(x, y, t) = Y_1(x, y)T(t)$ is the out-of-plane immersed deflection of FGM pates, and $Y_1(x, y)$ corresponds to its amplitude; t is the time. Eq. (5c) is the continuity condition of velocity at the fluid-plate interface. Using the method of separation of variables, the solution of φ induced by the vibration of rectangular plate is expressed as [46],

$$\varphi(x,y,z,t)=\sum_{l_1=1}^{\infty}\sum_{l_2=1}^{\infty}A_{l_1l_2}\cos(\lambda_1 x)\cos(\lambda_2 y)\mathrm{e}^{-\lambda_3|z|}\dot{T}(t), \tag{6}$$

where $\lambda_1 = (2l_1+1)\pi / 2L_1$, $\lambda_2 = l_2\pi / L_y$, $\lambda_3=-\sqrt{\lambda_1^2+\lambda_2^2}$, $l_1, l_2 = 0, 1, 2, \ldots$, $\dot{T}(t)=\mathrm{d}T(t)/\mathrm{d}t$, and

$$A_{l_1l_2}=\begin{cases}-\dfrac{c_{l_2}}{\lambda_3 L_1 L_y}\mathrm{e}^{\frac{\lambda_3 h_0}{2}}I(\lambda_1,\lambda_2), & y\ge\dfrac{h_0}{2},\\[2ex] \dfrac{c_{l_2}}{\lambda_3 L_1 L_y}\mathrm{e}^{\frac{\lambda_3 h_0}{2}}I(\lambda_1,\lambda_2), & y\le-\dfrac{h_0}{2},\end{cases}$$

with $I(\lambda_1,\lambda_2)=\int_0^{L_1}\int_0^{L_y}Y_1(x,y)\cos(\lambda_1 x)\cos(\lambda_2 y)\mathrm{d}x\mathrm{d}y$ and $c_{l_2}=\left\{\left(2,\text{ if } l_2=0\right),\ \left(4,\text{ if } l_2\neq 1\right)\right\}$.

Using the Bernoulli's equation [51,52]

$$P=-\rho_f\frac{\partial\varphi}{\partial t}, \tag{7}$$

the hydrodynamic pressure on any point P of the plate is solved. For FGM plates which contacted with fluid on one side, the resultant hydrodynamic pressure P_c projected on the z-axis is formulated as,

$$P_c(x,y,t)=P(x,y,\frac{h_0}{2},t)=\Theta_1(x,y)\frac{\partial^2 W_1}{\partial t^2}, \tag{8}$$

and for FGM plates which contacted with fluid on both sides, the hydrodynamic pressure P_c becomes,

$$P_c(x,y,t)=P(x,y,\frac{h_0}{2},t)-P(x,y,-\frac{h_0}{2},t)=\Theta_2(x,y)\frac{\partial^2 W_1}{\partial t^2}, \tag{9}$$

where

$$\Theta_1(x,y)=\Theta_2(x,y)/2, \tag{10a}$$

$$\Theta_2(x,y)=\begin{cases}\dfrac{2c_{l_2}\rho_f\cos(\lambda_1 x)\cos(\lambda_2 y)}{\lambda_3 L_1 L_y Y_1(x,y)}I(\lambda_1,\lambda_2), 0\le x\le L_1,\\ 0,\ \ L_1<x\le L.\end{cases} \tag{10b}$$

Note, $\Theta_1(x, y)$ and $\Theta_2(x, y)$ are the effective added masses on rectangular plates that caused by the fluid pressure for FGM plates contacted with fluid on one and two sides, respectively. Herein, $\Theta_1(x, y)$ and $\Theta_2(x, y)$ are dependent on the fluid density, immersed depth, plate characteristic scale and its vibrational modal.

2.2 Vibration of FGM plates

With the Mindlin plate theory [12], the displacements of FGM plates along *x*-, *y*- and *z*- axes are expressed as, respectively,

$$\tilde{U}(x,y,z,t)=U(x,y,t)+z\Psi_x(x,y,t), \tag{11}$$

$$\tilde{V}(x,y,z,t)=V(x,y,t)+z\Psi_y(x,y,t), \tag{12}$$

$$\tilde{W}(x,y,z,t)=W(x,y,t), \tag{13}$$

where $U(x, y, t)$, $V(x, y, t)$ and $W(x, y, t)$ refer to the corresponding displacements of mid-plane of FGM plates; $\Psi_x(x, y, t)$ and $\Psi_y(x, y, t)$ are the cross-sectional rotations about the *x*- and *y*- axes of lines normal to the middle plane before deformation. The nonzero components of strain are expressed as,

$$\begin{aligned}&\varepsilon_{xx}=\frac{\partial U}{\partial x}+z\frac{\partial \Psi_x}{\partial x},\ \varepsilon_{yy}=\frac{\partial V}{\partial y}+z\frac{\partial \Psi_y}{\partial y},\\ &\gamma_{xy}=\frac{\partial U}{\partial y}+\frac{\partial V}{\partial x}+z\left(\frac{\partial \Psi_x}{\partial y}+\frac{\partial \Psi_y}{\partial x}\right),\\ &\gamma_{xz}=\Psi_x+\frac{\partial W}{\partial x},\ \gamma_{yz}=\Psi_y+\frac{\partial W}{\partial y},\end{aligned} \tag{14}$$

The stresses are derived from the constitutive equation of stress-strain relationship

$$\sigma_{xx}=Q_{11}\varepsilon_{xx}+Q_{12}\varepsilon_{yy},\ \sigma_{yy}=Q_{11}\varepsilon_{yy}+Q_{12}\varepsilon_{xx}, \tag{15a}$$

$$\tau_{xy}=Q_{66}\gamma_{xy},\ \tau_{yz}=Q_{66}\gamma_{yz},\ \tau_{xz}=Q_{66}\gamma_{xz}, \tag{15b}$$

where

$$Q_{11}=\frac{E(z)}{1-\nu^2(z)},\ Q_{12}=\frac{\nu(z)E(z)}{1-\nu^2(z)},\ Q_{66}=\frac{E(z)}{2[1+\nu(z)]},$$

The internal forces are

$$\{N_{xx},N_{yy},N_{xy}\}=\int_{-h_0/2}^{h_0/2}\{\sigma_{xx},\sigma_{yy},\tau_{xy}\}\,\mathrm{d}z, \tag{16a}$$

$$\left\{M_{xx}, M_{yy}, M_{xy}\right\} = \int_{-h_0/2}^{h_0/2} \left\{\sigma_{xx}, \sigma_{yy}, \tau_{xy}\right\} z\mathrm{d}z, \tag{16b}$$

$$\left\{Q_x, Q_y\right\} = \kappa \int_{-h_0/2}^{h_0/2} \left\{\tau_{xz}, \tau_{yz}\right\} \mathrm{d}z, \tag{16c}$$

The stiffness components and inertia terms are defined as

$$\left\{A_{11}, A_{12}, A_{66}\right\} = \int_{-h_0/2}^{h_0/2} \left\{Q_{11}, Q_{12}, Q_{66}\right\} \mathrm{d}z, \ \left\{B_{11}, B_{12}, B_{66}\right\} = \int_{-h_0/2}^{h_0/2} \left\{Q_{11}, Q_{12}, Q_{66}\right\} z\mathrm{d}z,$$
$$\left\{D_{11}, D_{12}, D_{66}\right\} = \int_{-h_0/2}^{h_0/2} \left\{Q_{11}, Q_{12}, Q_{66}\right\} z^2\mathrm{d}z, \ \left\{I_1, I_2, I_3\right\} = \int_{-h_0/2}^{h_0/2} \rho(z)\left\{1, z, z^2\right\} \mathrm{d}z.$$

where the shear correction factor of the FGM plate κ = 5/6. Indeed, for FGM plate, the shear correction factor is also function of z, and can be accurately expressed as $\kappa = \dfrac{5}{6-\left(v_a V_1 + v_b V_2\right)}$ where V_1 and V_2 are the volume fraction of the metal and ceramic in the entire cross-section, respectively [53]. However, $5/6$ or $\pi^2/12$ is well accepted as the approximate value of the shear correction factor for FGM beams and plates with the rectangular cross section. Therefore, it is reasonable to used value 5/6.

The potential energy Π_S of this plate-fluid coupling system is:

$$\begin{aligned}
\Pi_S &= \frac{1}{2}\int_0^{L_y}\int_0^{L_x}\left(\sigma_{xx}\varepsilon_{xx} + \sigma_{yy}\varepsilon_{yy} + \tau_{xy}\gamma_{xy} + \tau_{xz}\gamma_{xz} + \tau_{yz}\gamma_{yz}\right)\mathrm{d}x\mathrm{d}y \\
&= \frac{1}{2}\int_0^{L_y}\int_0^{L_1}\left[N_{xx1}\frac{\partial U_1}{\partial x_1} + N_{yy1}\frac{\partial V_1}{\partial y} + N_{xy1}\left(\frac{\partial U_1}{\partial y} + \frac{\partial V_1}{\partial x_1}\right) + M_{xx1}\frac{\partial \Psi_{x1}}{\partial x_1} + M_{yy1}\frac{\partial \Psi_{y1}}{\partial y}\right. \\
&\qquad \left. + M_{xy1}\left(\frac{\partial \Psi_{x1}}{\partial y} + \frac{\partial \Psi_{y1}}{\partial x_1}\right) + Q_{x1}\left(\Psi_{x1} + \frac{\partial W_1}{\partial x_1}\right) + Q_{y1}\left(\Psi_{x1} + \frac{\partial W_1}{\partial x_1}\right)\right]\mathrm{d}x_1\mathrm{d}y \\
&\quad + \frac{1}{2}\int_0^{L_y}\int_{L_1}^{L_x}\left[N_{xx2}\frac{\partial U_2}{\partial x_2} + N_{yy2}\frac{\partial V_2}{\partial y} + N_{xy2}\left(\frac{\partial U_2}{\partial y} + \frac{\partial V_2}{\partial x_2}\right) + M_{xx2}\frac{\partial \Psi_{x2}}{\partial x_2} + M_{yy2}\frac{\partial \Psi_{y2}}{\partial y}\right. \\
&\qquad \left. + M_{xy2}\left(\frac{\partial \Psi_{x2}}{\partial y} + \frac{\partial \Psi_{y2}}{\partial x_2}\right) + Q_{x2}\left(\Psi_{x2} + \frac{\partial W_2}{\partial x_2}\right) + Q_{y2}\left(\Psi_{x2} + \frac{\partial W_2}{\partial x_2}\right)\right]\mathrm{d}x_2\mathrm{d}y.
\end{aligned} \tag{17}$$

The kinetic energy Π_T is:

$$\begin{aligned}
\Pi_T &= \frac{1}{2}\int_0^{L_y}\int_0^{L_1}\left\{I_1\left[\left(\frac{\partial U_1}{\partial t}\right)^2 + \left(\frac{\partial V_1}{\partial t}\right)^2 + \left(\frac{\partial W_1}{\partial t}\right)^2\right] + 2I_2\left[\frac{\partial U_1}{\partial t}\frac{\partial \Psi_{x1}}{\partial t} + \frac{\partial V_1}{\partial t}\frac{\partial \Psi_{y1}}{\partial t}\right]\right. \\
&\quad \left. + I_3\left[\left(\frac{\partial \Psi_{x1}}{\partial t}\right)^2 + \left(\frac{\partial \Psi_{y1}}{\partial t}\right)^2\right]\right\}\mathrm{d}x_1\mathrm{d}y + \frac{1}{2}\int_0^{L_y}\int_{L_1}^{L_x}\left\{I_1\left[\left(\frac{\partial U_2}{\partial t}\right)^2 + \left(\frac{\partial V_2}{\partial t}\right)^2 + \left(\frac{\partial W_2}{\partial t}\right)^2\right]\right. \\
&\quad \left. + 2I_2\left[\frac{\partial U_2}{\partial t}\frac{\partial \Psi_{x2}}{\partial t} + \frac{\partial V_2}{\partial t}\frac{\partial \Psi_{y2}}{\partial t}\right] + I_3\left[\left(\frac{\partial \Psi_{x2}}{\partial t}\right)^2 + \left(\frac{\partial \Psi_{y2}}{\partial t}\right)^2\right]\right\}\mathrm{d}x_2\mathrm{d}y.
\end{aligned} \tag{18}$$

$F(x, y, t)$ is the fluid-loading force, which is interacting with the resultant hydrodynamic pressure $P_c(x, y, t)$ for

rectangular FGM plates. The work of fluid force Π_F is:

$$\Pi_F = \int_0^{L_1} F(x, y, t) W_1 \mathrm{d}x_1 \mathrm{d}y, \tag{19}$$

where $$F(x, y, t) = -P_c(x, y, t) = -\Theta(x_i, y) \frac{\partial^2 W_1}{\partial t^2},$$

$\Theta(x_i, y)$ is the added mass of FGM plates, which is replaced by $\Theta_1(x_i, y)$ and $\Theta_2(x_i, y)$ given by Eq. (10) for FGM plates contacted with fluid on one and two sides, respectively; $x_1 \in [0, L_1]$ and $x_2 \in [L_1, L_x]$ corresponds to the bottom and top sub-plate separated by the free surface of fluid, respectively.

Applying the Hamilton's principle,

$$\int_0^t (\delta\Pi_T - \delta\Pi_S + \delta\Pi_F) \mathrm{d}t = 0, \tag{20}$$

the governing equations of the plate-fluid system are obtained using the method of integration by parts

$$\frac{\partial N_{xxi}}{\partial x_i} + \frac{\partial N_{xyi}}{\partial y} = I_1 \frac{\partial^2 U_i}{\partial t^2} + I_2 \frac{\partial^2 \Psi_{xi}}{\partial t^2}, \tag{21}$$

$$\frac{\partial N_{xyi}}{\partial x_i} + \frac{\partial N_{yyi}}{\partial y} = I_1 \frac{\partial^2 V_i}{\partial t^2} + I_2 \frac{\partial^2 \Psi_{yi}}{\partial t^2}, \tag{22}$$

$$\frac{\partial Q_{xi}}{\partial x_i} + \frac{\partial Q_{yi}}{\partial y} = I_1 \frac{\partial^2 W_i}{\partial t^2} + \Theta(x_i, y) \frac{\partial^2 W_i}{\partial t^2}, \tag{23}$$

$$\frac{\partial M_{xxi}}{\partial x_i} + \frac{\partial M_{xyi}}{\partial y} - Q_{xi} = I_2 \frac{\partial^2 U_i}{\partial t^2} + I_3 \frac{\partial^2 \Psi_{xi}}{\partial t^2}, \tag{24}$$

$$\frac{\partial M_{xyi}}{\partial x_i} + \frac{\partial M_{yyi}}{\partial y} - Q_{yi} = I_2 \frac{\partial^2 V_i}{\partial t^2} + I_3 \frac{\partial^2 \Psi_{yi}}{\partial t^2}, \tag{25}$$

where subscripts $i = 1$ and $i = 2$ represent the corresponding physical quantities on the bottom and top sub-plate separated by fluid free surface, respectively. The boundary conditions of FGM plates require

$$\begin{aligned} &U_i = 0 \text{ or } N_{xxi} = 0, \; V_i = 0 \text{ or } N_{xyi} = 0, \\ &W_i = 0 \text{ or } Q_{xi} = 0, \; \Psi_{xi} = 0 \text{ or } M_{xxi} = 0, \\ &\Psi_{yi} = 0 \text{ or } M_{xyi} = 0, \end{aligned} \tag{26}$$

at $x_1 = 0$ and $x_2 = L_x$;

$$\begin{aligned} &U_i = 0 \text{ or } N_{xyi} = 0, \; V_i = 0 \text{ or } N_{yyi} = 0, \\ &W_i = 0 \text{ or } Q_{yi} = 0, \; \Psi_{xi} = 0 \text{ or } M_{xyi} = 0, \\ &\Psi_{yi} = 0 \text{ or } M_{yyi} = 0, \end{aligned} \tag{27}$$

at $y = 0$ and $y = L_y$;

$$\begin{aligned} &U_1 = U_2,\ V_1 = V_2,\ W_1 = W_2, \\ &\Psi_{x1} = \Psi_{x2},\ \Psi_{y1} = \Psi_{y2},\ Q_{x1} = Q_{x2}, \\ &N_{xx1} = N_{xx2},\ N_{xy1} = N_{xy2}, \\ &M_{xx1} = M_{xx2},\ M_{xy1} = M_{xy2}, \end{aligned} \tag{28}$$

at $x_1 = L_1$.

The following non-dimensional parameters are introduced:

$$\begin{aligned} &(u_i, v_i, w_i) = \frac{(U_i, V_i, W_i)}{h_0},\ (\psi_{xi}, \psi_{yi}) = (\Psi_{xi}, \Psi_{yi}), \\ &(\zeta_1, \zeta_2, \zeta) = \left(\frac{x_1}{L_1}, \frac{x_2 - L_1}{L_x - L_1}, \frac{x}{L_x} \right),\ \xi = \frac{y}{L_y}, \end{aligned} \tag{29a}$$

$$\begin{aligned} &(\eta_1, \eta_2, \eta_0) = \frac{(L_1, L_x - L_1, L_x)}{h_0},\ (g_1, g_2) = \frac{(L_1, L_x - L_1)}{L_x}, \\ &\left(a_{11}, a_{12}, a_{66}\right) = \frac{(A_{11}, A_{12}, A_{66})}{A_{110}},\ (\lambda_1, \lambda_2) = \frac{(L_1, L_x - L_1)}{L_y}, \end{aligned} \tag{29b}$$

$$\begin{aligned} &\left(b_{11}, b_{12}, b_{66}\right) = \frac{(B_{11}, B_{12}, B_{66})}{A_{110} h_0},\ \ (m_{f1}, m_{f2}) = \frac{(\Theta_1, \Theta_2)}{I_{10}}, \\ &\left(d_{11}, d_{12}, d_{66}\right) = \frac{(D_{11}, D_{12}, D_{66})}{A_{110} h_0^2},\ \omega = \Omega L_x \sqrt{\frac{I_{10}}{A_{110}}}, \end{aligned} \tag{29c}$$

$$\left(\bar{I}_1, \bar{I}_2, \bar{I}_3\right) = \left(\frac{I_1}{I_{10}}, \frac{I_2}{I_{10} h_0}, \frac{I_3}{I_{10} h_0^2} \right),\ \tau = \frac{t}{L_x} \sqrt{\frac{A_{110}}{I_{10}}}, \tag{29d}$$

where I_{10} and A_{110} are equal to I_1 and A_{11} of homogeneous plates, respectively; η_0 defines the slenderness ratio; m_{f1} and m_{f2} are normalized added mass of FGM plates contacted with fluid on one and two sides, respectively; g_1 represents the dimensionless immersed depth; ω corresponds to the dimensionless form of the angular frequency Ω.

The dimensionless forms of Eqs. (21)-(25) are

$$\begin{aligned} &a_{11} \frac{\partial^2 u_i}{\partial \zeta_i^{\,2}} + b_{11} \frac{\partial^2 \psi_{xi}}{\partial \zeta_i^{\,2}} + \lambda_i (a_{12} + a_{66}) \frac{\partial^2 v_i}{\partial \zeta_i \partial \xi} + \lambda_i (b_{12} + b_{66}) \frac{\partial^2 \psi_{yi}}{\partial \zeta_i \partial \xi} \\ &+ \lambda_i^{\,2} a_{66} \frac{\partial^2 u_i}{\partial \xi^2} + \lambda_i^{\,2} b_{66} \frac{\partial^2 \psi_{xi}}{\partial \xi^2} = g_i^{\,2} \left[\bar{I}_1 \frac{\partial^2 u_i}{\partial \tau^2} + \bar{I}_2 \frac{\partial^2 \psi_{xi}}{\partial \tau^2} \right], \end{aligned} \tag{30}$$

$$\begin{aligned} &a_{66} \frac{\partial^2 v_i}{\partial \zeta_i^{\,2}} + b_{66} \frac{\partial^2 \psi_{yi}}{\partial \zeta_i^{\,2}} + \lambda_i (a_{12} + a_{66}) \frac{\partial^2 u_i}{\partial \zeta_i \partial \xi} + \lambda_i (b_{12} + b_{66}) \frac{\partial^2 \psi_{xi}}{\partial \zeta_i \partial \xi} \\ &+ \lambda_i^{\,2} a_{11} \frac{\partial^2 v_i}{\partial \xi^2} + \lambda_i^{\,2} b_{11} \frac{\partial^2 \psi_{yi}}{\partial \xi^2} = g_i^{\,2} \left[\bar{I}_1 \frac{\partial^2 v_i}{\partial \tau^2} + \bar{I}_2 \frac{\partial^2 \psi_{yi}}{\partial \tau^2} \right], \end{aligned} \tag{31}$$

$$\kappa a_{66}\left(\frac{\partial^2 w_i}{\partial \zeta_i^{\,2}}+\eta_i\frac{\partial \psi_{xi}}{\partial \zeta_i}+\eta_i\lambda_i\frac{\partial \psi_{yi}}{\partial \xi_i}+\lambda_i^{\,2}\frac{\partial^2 w_i}{\partial \xi_i^{\,2}}\right)=g_i^{\,2}\left[\bar{I}_1+m_f(\zeta_i,\xi)\right]\frac{\partial^2 w_i}{\partial \tau^2}, \tag{32}$$

$$\begin{aligned}&b_{11}\frac{\partial^2 u_i}{\partial \zeta_i^{\,2}}+d_{11}\frac{\partial^2 \psi_{xi}}{\partial \zeta_i^{\,2}}+\lambda_i(b_{12}+b_{66})\frac{\partial^2 v_i}{\partial \zeta_i \partial \xi}+\lambda_i(d_{12}+d_{66})\frac{\partial^2 \psi_{yi}}{\partial \zeta_i \partial \xi}+\lambda_i^{\,2}b_{66}\frac{\partial^2 u_i}{\partial \xi^2}\\&+\lambda_i^{\,2}d_{66}\frac{\partial^2 \psi_{xi}}{\partial \xi^2}-\kappa a_{66}\left(\eta_i^{\,2}\psi_{xi}+\eta_i\frac{\partial w_i}{\partial \zeta_i}\right)=g_i^{\,2}\left[\bar{I}_2\frac{\partial^2 u_i}{\partial \tau^2}+\bar{I}_3\frac{\partial^2 \psi_{xi}}{\partial \tau^2}\right],\end{aligned} \tag{33}$$

$$\begin{aligned}&b_{66}\frac{\partial^2 v_i}{\partial \zeta_i^{\,2}}+d_{66}\frac{\partial^2 \psi_{yi}}{\partial \zeta_i^{\,2}}+\lambda_i(b_{12}+b_{66})\frac{\partial^2 u_i}{\partial \zeta_i \partial \xi}+\lambda_i(d_{12}+d_{66})\frac{\partial^2 \psi_{xi}}{\partial \zeta_i \partial \xi}+\lambda_i^{\,2}b_{11}\frac{\partial^2 v_i}{\partial \xi^2}\\&+\lambda_i^{\,2}d_{11}\frac{\partial^2 \psi_{yi}}{\partial \xi^2}-\kappa a_{66}\left(\eta_i^{\,2}\psi_{yi}+\eta_i\frac{\partial w_i}{\partial \xi}\right)=g_i^{\,2}\left[\bar{I}_2\frac{\partial^2 v_i}{\partial \tau^2}+\bar{I}_3\frac{\partial^2 \psi_{yi}}{\partial \tau^2}\right],\end{aligned} \tag{34}$$

where i = 1 and 2; $m_f(\zeta_i, \xi) = m_{f1}(\zeta_i, \xi)$ and $m_f(\zeta_i, \xi) = m_{f2}(\zeta_i, \xi)$ refer to FGM plates contacted with fluid on one and both sides, respectively. The non-dimensional boundary conditions are:

$$u_i = v_i = w_i = \psi_{xi} = \psi_{yi} = 0, \text{ at } \zeta_1 = 0 \text{ and } \zeta_2 = 1, \tag{35a}$$

$$u_i = v_i = w_i = \psi_{xi} = \psi_{yi} = 0, \text{ at } \xi = 0 \text{ and } \xi = 1, \tag{35b}$$

for a plate with all edges clamped (CCCC), and the boundary conditions are expressed as,

$$\begin{aligned}&u_i = v_i = w_i = \psi_{yi} = 0,\\&b_{11}\frac{\partial u_i}{\partial \zeta_i}+d_{11}\frac{\partial \psi_{xi}}{\partial \zeta_i}+\lambda_i b_{12}\frac{\partial v_i}{\partial \xi}+\lambda_i d_{12}\frac{\partial \psi_{yi}}{\partial \xi}=0,\\&\text{at } \zeta_1 = 0 \text{ and } \zeta_2 = 1,\end{aligned} \tag{36a}$$

$$\begin{aligned}&u_i = v_i = w_i = \psi_{xi} = 0,\\&b_{12}\frac{\partial u_i}{\partial \zeta_i}+d_{12}\frac{\partial \psi_{xi}}{\partial \zeta_i}+\lambda_i b_{11}\frac{\partial v_i}{\partial \xi}+\lambda_i d_{11}\frac{\partial \psi_{yi}}{\partial \xi}=0,\\&\text{at } \xi = 0 \text{ and } \xi = 1,\end{aligned} \tag{36a}$$

for a plate with all edges simply-supported (SSSS), and the boundary conditions are expressed as,

$$u_1 = v_1 = w_1 = \psi_{x1} = \psi_{y1} = 0, \text{ at } \zeta_1 = 0, \tag{37a}$$

$$
\begin{aligned}
&a_{11}\frac{\partial u_2}{\partial \zeta_2}+b_{11}\frac{\partial \psi_{x2}}{\partial \zeta_2}+\lambda_2 a_{12}\frac{\partial v_2}{\partial \xi}+\lambda_2 b_{12}\frac{\partial \psi_{y2}}{\partial \xi}=0,\\
&b_{11}\frac{\partial u_2}{\partial \zeta_2}+d_{11}\frac{\partial \psi_{x2}}{\partial \zeta_2}+\lambda_2 b_{12}\frac{\partial v_2}{\partial \xi}+\lambda_2 d_{12}\frac{\partial \psi_{y2}}{\partial \xi}=0,\\
&a_{66}\frac{\partial v_2}{\partial \zeta_2}+b_{66}\frac{\partial \psi_{y2}}{\partial \zeta_2}+\lambda_2 a_{66}\frac{\partial u_2}{\partial \xi}+\lambda_2 b_{66}\frac{\partial \psi_{x2}}{\partial \xi}=0,\\
&b_{66}\frac{\partial v_2}{\partial \zeta_2}+d_{66}\frac{\partial \psi_{y2}}{\partial \zeta_2}+\lambda_2 b_{66}\frac{\partial u_2}{\partial \xi}+\lambda_2 d_{66}\frac{\partial \psi_{x2}}{\partial \xi}=0,\\
&\kappa a_{66}\left(\eta_2\psi_{x2}+\frac{\partial w_2}{\partial \zeta_2}\right)=0,\ \text{at}\ \ \zeta_1=1,
\end{aligned}
\tag{37b}
$$

$$
\begin{aligned}
&a_{12}\frac{\partial u_i}{\partial \zeta_i}+b_{12}\frac{\partial \psi_{xi}}{\partial \zeta_i}+\lambda_i a_{11}\frac{\partial v_i}{\partial \xi}+\lambda_i b_{11}\frac{\partial \psi_{yi}}{\partial \xi}=0,\\
&b_{12}\frac{\partial u_i}{\partial \zeta_i}+d_{12}\frac{\partial \psi_{xi}}{\partial \zeta_i}+\lambda_i b_{11}\frac{\partial v_i}{\partial \xi}+\lambda_i d_{11}\frac{\partial \psi_{yi}}{\partial \xi}=0,\\
&a_{66}\frac{\partial v_i}{\partial \zeta_i}+b_{66}\frac{\partial \psi_{yi}}{\partial \zeta_i}+\lambda_i a_{66}\frac{\partial u_i}{\partial \xi}+\lambda_i b_{66}\frac{\partial \psi_{xi}}{\partial \xi}=0,\\
&b_{66}\frac{\partial v_i}{\partial \zeta_i}+d_{66}\frac{\partial \psi_{yi}}{\partial \zeta_i}+\lambda_i b_{66}\frac{\partial u_i}{\partial \xi}+\lambda_i d_{66}\frac{\partial \psi_{xi}}{\partial \xi}=0,\\
&\kappa a_{66}\left(\eta_i\psi_{yi}+\lambda_i\frac{\partial w_i}{\partial \xi}\right)=0,\ \text{at}\ \xi=0\ \text{and}\ \xi=1,
\end{aligned}
\tag{37c}
$$

for a cantilever plate (CFFF). At $\zeta_1 = 1$, the following conditions should be satisfied

$$
u_1=u_2,\ v_1=v_2,\ w_1=w_2,\ \psi_{x1}=\psi_{x2},\ \psi_{y1}=\psi_{y2},
\tag{38a}
$$

$$
\begin{aligned}
&\frac{a_{11}}{\lambda_1}\frac{\partial u_1}{\partial \zeta_1}+\frac{b_{11}}{\lambda_1}\frac{\partial \psi_{x1}}{\partial \zeta_1}+a_{12}\frac{\partial v_1}{\partial \xi}+b_{12}\frac{\partial \psi_{y1}}{\partial \xi}\\
&=\frac{a_{11}}{\lambda_2}\frac{\partial u_2}{\partial \zeta_2}+\frac{b_{11}}{\lambda_2}\frac{\partial \psi_{x2}}{\partial \zeta_2}+a_{12}\frac{\partial v_2}{\partial \xi}+b_{12}\frac{\partial \psi_{y2}}{\partial \xi},
\end{aligned}
\tag{38b}
$$

$$
\begin{aligned}
&\frac{b_{11}}{\lambda_1}\frac{\partial u_1}{\partial \zeta_1}+\frac{d_{11}}{\lambda_1}\frac{\partial \psi_{x1}}{\partial \zeta_1}+b_{12}\frac{\partial v_1}{\partial \xi}+d_{12}\frac{\partial \psi_{y1}}{\partial \xi}\\
&=\frac{b_{11}}{\lambda_2}\frac{\partial u_2}{\partial \zeta_2}+\frac{d_{11}}{\lambda_2}\frac{\partial \psi_{x2}}{\partial \zeta_2}+b_{12}\frac{\partial v_2}{\partial \xi}+d_{12}\frac{\partial \psi_{y2}}{\partial \xi},
\end{aligned}
\tag{38c}
$$

$$
\begin{aligned}
&\frac{a_{66}}{\lambda_1}\frac{\partial v_1}{\partial \zeta_1}+\frac{b_{66}}{\lambda_1}\frac{\partial \psi_{y1}}{\partial \zeta_1}+a_{66}\frac{\partial u_1}{\partial \xi}+b_{66}\frac{\partial \psi_{x1}}{\partial \xi}\\
&=\frac{a_{66}}{\lambda_2}\frac{\partial v_2}{\partial \zeta_2}+\frac{b_{66}}{\lambda_2}\frac{\partial \psi_{y2}}{\partial \zeta_2}+a_{66}\frac{\partial u_2}{\partial \xi}+b_{66}\frac{\partial \psi_{x2}}{\partial \xi},
\end{aligned}
\tag{38d}
$$

$$\frac{b_{66}}{\lambda_1}\frac{\partial v_1}{\partial \zeta_1}+\frac{d_{66}}{\lambda_1}\frac{\partial \psi_1}{\partial \zeta_1}+b_{66}\frac{\partial u_1}{\partial \xi}+d_{66}\frac{\partial \psi_{x1}}{\partial \xi}$$
$$=\frac{b_{66}}{\lambda_2}\frac{\partial v_2}{\partial \zeta_2}+\frac{d_{66}}{\lambda_2}\frac{\partial \psi_{y2}}{\partial \zeta_2}+b_{66}\frac{\partial u_2}{\partial \xi}+d_{66}\frac{\partial \psi_{x2}}{\partial \xi}, \tag{38e}$$

$$\eta_1\psi_{x1}+\frac{\partial w_1}{\partial \zeta_1}=\eta_2\psi_{x2}+\frac{\partial w_2}{\partial \zeta_2}. \tag{38f}$$

2.3 Solution method

The differential quadrature (DQ) method is applied to simplify Eqs. (30)-(38) through discretizing unknown variables u_i, v_i, w_i, ψ_{xi}, ψ_{yi} and their kth derivatives as,

$$\left\{u_i, v_i, w_i, \psi_{xi}, \psi_{yi}\right\}$$
$$=\sum_{n=1}^{N}\sum_{m=1}^{M} l_n(\zeta_i) l_m(\xi)\left\{u_{i,mn}, v_{i,mn}, w_{i,mn}, \psi_{xi,mn}, \psi_{yi,mn}\right\}\Big|_{\zeta=\zeta_{i,n},\xi=\xi_m}, \tag{39a}$$

$$\frac{\partial^{k_1}}{\partial \xi^{k_1}}\frac{\partial^{k_2}}{\partial \zeta_i^{k_2}}\left\{u_i, v_i, w_i, \psi_{xi}, \psi_{yi}\right\}$$
$$=\sum_{n=1}^{N}\sum_{m=1}^{M} C_m^{k_1}(\xi) C_n^{k_2}(\zeta_i)\left\{u_{imn}, v_{imn}, w_{imn}, \psi_{ximn}, \psi_{yimn}\right\}\Big|_{\zeta=\zeta_{i,n},\xi=\xi_m}, \tag{39b}$$

where N and M sampling points of each sub-plate along x and y axes, respectively. According to the Chebyshev–Gauss–Lobatto distribution [54], sampling points are formulated as

$$\zeta_{ik_1}=\frac{1}{2}\left\{1-\cos\left[\frac{\pi(k_1-1)}{N-1}\right]\right\},\ k_1=1, 2, \ldots N, \tag{40a}$$

$$\xi_{k_2}=\frac{1}{2}\left\{1-\cos\left[\frac{\pi(k_2-1)}{M-1}\right]\right\},\ k_2=1, 2, \ldots M, \tag{40b}$$

where ζ_{ik_1} and ξ_{k_2} are the values of k_1th and k_2th sampling points on the ζ_i- and ξ- axis, respectively; { u_{imn}, v_{imn}, w_{imn}, ψ_{ximn}, ψ_{yimn} }= {$u(\zeta_{in}, \xi_m, t)$, $v(\zeta_{in}, \xi_m, t)$, $w(\zeta_{in}, \xi_m, t)$, $\psi_x(\zeta_{in}, \xi_m, t)$, $\psi_y(\zeta_{in}, \xi_m, t)$}; $l_n(\zeta_i)$, $l_m(\xi)$, and $C_m^{k_1}(\xi)$, $C_n^{k_2}(\zeta_i)$ respectively refer to the Lagrange interpolation polynomials and weighted coefficient obtained in Shu [54].

Then, Eqs. (30)-(34) are discretized as

$$a_{11}\sum_{n=1}^{N} C_{k_1n}^{(2)} u_{ink_2}+b_{11}\sum_{n=1}^{N} C_{k_1n}^{(2)}\psi_{xink_2}+\lambda_i(a_{12}+a_{66})\sum_{n=1}^{N}\sum_{m=1}^{M} C_{k_1n}^{(1)} C_{k_2m}^{(1)} v_{inm}$$
$$+\lambda_i(b_{12}+b_{66})\sum_{n=1}^{N}\sum_{m=1}^{M} C_{k_1n}^{(1)} C_{k_2m}^{(1)}\psi_{yinm}+\lambda_i^{\,2} a_{66}\sum_{m=1}^{M} C_{k_2m}^{(2)} u_{ik_1m} \tag{41}$$
$$+\lambda_i^{\,2} b_{66}\sum_{m=1}^{M} C_{k_2m}^{(2)}\psi_{xik_1m}=g_i^{\,2}\left[\bar{I}_1\ddot{u}_{ik_1k_2}+\bar{I}_2\ddot{\psi}_{xik_1k_2}\right],$$

$$
\begin{aligned}
&a_{66}\sum_{n=1}^{N}C_{k_1n}^{(2)}v_{ink_2}+b_{66}\sum_{n=1}^{N}C_{k_1n}^{(2)}\psi_{yink_2}+\lambda_i(a_{12}+a_{66})\sum_{n=1}^{N}\sum_{m=1}^{M}C_{k_1n}^{(1)}C_{k_2m}^{(1)}u_{inm}\\
&+\lambda_i(b_{12}+b_{66})\sum_{n=1}^{N}\sum_{m=1}^{M}C_{k_1n}^{(1)}C_{k_2m}^{(1)}\psi_{xinm}+\lambda_i^{\,2}a_{11}\sum_{m=1}^{M}C_{k_2m}^{(2)}v_{ik_1m}\\
&+\lambda_i^{\,2}b_{11}\sum_{m=1}^{M}C_{k_2m}^{(2)}\psi_{yik_1m}=g_i^{\,2}\left[\bar{I}_1\ddot{v}_{ik_1k_2}+\bar{I}_2\ddot{\psi}_{yik_1k_2}\right],
\end{aligned}
\tag{42}
$$

$$
\begin{aligned}
&\kappa a_{66}\left(\sum_{n=1}^{N}C_{k_1n}^{(2)}w_{ink_2}+\eta_i\sum_{n=1}^{N}C_{k_1n}^{(1)}\psi_{xink_2}+\eta_i\lambda_i\sum_{m=1}^{M}C_{k_2m}^{(1)}\psi_{yik_1m}\right.\\
&\left.+\lambda_i^{\,2}\sum_{m=1}^{M}C_{k_2m}^{(2)}w_{ik_1m}\right)=g_i^{\,2}\left[\bar{I}_1+m_f(\zeta_i,\xi)\right]\ddot{w}_{ik_1k_2},
\end{aligned}
\tag{43}
$$

$$
\begin{aligned}
&b_{11}\sum_{n=1}^{N}C_{k_1n}^{(2)}u_{ink_2}+d_{11}\sum_{n=1}^{N}C_{k_1n}^{(2)}\psi_{xink_2}+\lambda_i(b_{12}+b_{66})\sum_{n=1}^{N}\sum_{m=1}^{M}C_{k_1n}^{(1)}C_{k_2m}^{(1)}v_{inm}\\
&+\lambda_i(d_{12}+d_{66})\sum_{n=1}^{N}\sum_{m=1}^{M}C_{k_1n}^{(1)}C_{k_2m}^{(1)}\psi_{yinm}+\lambda_i^{\,2}b_{66}\sum_{m=1}^{M}C_{k_2m}^{(2)}u_{ik_1m}+\lambda_i^{\,2}d_{66}\sum_{m=1}^{M}C_{k_2m}^{(2)}\psi_{xik_1m}\\
&-\kappa a_{66}\left(\eta_i^{\,2}\psi_{xik_1k_2}+\eta_i\sum_{n=1}^{N}C_{k_1n}^{(1)}w_{ink_2}\right)=g_i^{\,2}\left[\bar{I}_2\ddot{u}_{ik_1k_2}+\bar{I}_3\ddot{\psi}_{xik_1k_2}\right],
\end{aligned}
\tag{44}
$$

$$
\begin{aligned}
&b_{66}\sum_{n=1}^{N}C_{k_1n}^{(2)}v_{ink_2}+d_{66}\sum_{n=1}^{N}C_{k_1n}^{(2)}\psi_{yink_2}+\lambda_i(b_{12}+b_{66})\sum_{n=1}^{N}\sum_{m=1}^{M}C_{k_1n}^{(1)}C_{k_2m}^{(1)}u_{inm}\\
&+\lambda_i(d_{12}+d_{66})\sum_{n=1}^{N}\sum_{m=1}^{M}C_{k_1n}^{(1)}C_{k_2m}^{(1)}\psi_{xinm}+\lambda_i^{\,2}b_{11}\sum_{m=1}^{M}C_{k_2m}^{(2)}v_{ik_1m}+\lambda_i^{\,2}d_{11}\sum_{m=1}^{M}C_{k_2m}^{(2)}\psi_{yik_1m}\\
&-\kappa a_{66}\left(\eta_i^{\,2}\psi_{yik_1k_2}+\eta_i\lambda_i\sum_{m=1}^{M}C_{k_2m}^{(1)}w_{ik_1m}\right)=g_i^{\,2}\left[\bar{I}_2\ddot{v}_{ik_1k_2}+\bar{I}_3\ddot{\psi}_{yik_1k_2}\right],
\end{aligned}
\tag{45}
$$

where $i = 1, 2$. The dimensionless boundary conditions are given by,

$$
\begin{aligned}
&u_{ik_1k_2}=v_{ik_1k_2}=w_{ik_1k_2}=\psi_{xik_1k_2}=\psi_{yik_1k_2}=0,\\
&\text{at }\ \zeta_{11}=0,\ \zeta_{2N}=1,\ \ \xi_1=0 \text{ and } \xi_M=1,
\end{aligned}
\tag{46}
$$

for a CCCC plate, the dimensionless boundary conditions are expressed as,

$$
\begin{aligned}
&u_{ik_1k_2}=v_{ik_1k_2}=w_{ik_1k_2}=\psi_{yik_1k_2}=0,\\
&b_{11}\sum_{n=1}^{N}C_{k_1n}^{(1)}u_{ink_2}+d_{11}\sum_{n=1}^{N}C_{k_1n}^{(1)}\psi_{xink_2}+\lambda_i b_{12}\sum_{m=1}^{M}C_{k_2m}^{(1)}v_{ik_1m}\\
&+\lambda_i d_{12}\sum_{m=1}^{M}C_{k_2m}^{(1)}\psi_{yik_1m}=0,\ \text{at }\ \zeta_{11}=0 \text{ and } \zeta_{2N}=1,
\end{aligned}
\tag{47a}
$$

$$
\begin{aligned}
&u_{ik_1k_2}=v_{ik_1k_2}=w_{ik_1k_2}=\psi_{xik_1k_2}=0,\\
&b_{12}\sum_{n=1}^{N}C_{k_1n}^{(1)}u_{ink_2}+d_{12}\sum_{n=1}^{N}C_{k_1n}^{(1)}\psi_{xink_2}+\lambda_i b_{11}\sum_{m=1}^{M}C_{k_2m}^{(1)}v_{ik_1m}\\
&+\lambda_i d_{11}\sum_{m=1}^{M}C_{k_2m}^{(1)}\psi_{yik_1m}=0,\ \text{at } \xi_1=0 \text{ and } \xi_M=1,
\end{aligned}
\tag{47b}
$$

for a SSSS plate, the boundary conditions are,

$$u_{11k_2} = v_{11k_2} = w_{11k_2} = \psi_{x11k_2} = \psi_{y11k_2} = 0, \text{ at } \zeta_{11}=0, \tag{48a}$$

$$\begin{aligned}
&a_{11}\sum_{n=1}^{N} C_{Nn}^{(1)} u_{2Nk_2} + b_{11}\sum_{n=1}^{N} C_{Nn}^{(1)} \psi_{x2Nk_2} + \lambda_2 a_{12}\sum_{m=1}^{M} C_{k_2m}^{(1)} \psi_{x2k_1m} + \lambda_2 b_{12}\sum_{m=1}^{M} C_{k_2m}^{(1)} \psi_{y2k_1m} = 0 \\
&b_{11}\sum_{n=1}^{N} C_{Nn}^{(1)} u_{2Nk_2} + \mathrm{d}_{11}\sum_{n=1}^{N} C_{Nn}^{(1)} \psi_{x2Nk_2} + \lambda_2 b_{12}\sum_{m=1}^{M} C_{k_2m}^{(1)} \psi_{x2k_1m} + \lambda_2 d_{12}\sum_{m=1}^{M} C_{k_2m}^{(1)} \psi_{y2k_1m} = 0 \\
&a_{66}\sum_{n=1}^{N} C_{Nn}^{(1)} v_{2Nk_2} + b_{66}\sum_{n=1}^{N} C_{Nn}^{(1)} \psi_{y2Nk_2} + \lambda_2 a_{66}\sum_{m=1}^{M} C_{k_2m}^{(1)} u_{2k_1m} + \lambda_2 b_{66}\sum_{m=1}^{M} C_{k_2m}^{(1)} \psi_{x2k_1m} = 0, \\
&b_{66}\sum_{n=1}^{N} C_{Nn}^{(1)} v_{2Nk_2} + d_{66}\sum_{n=1}^{N} C_{Nn}^{(1)} \psi_{y2Nk_2} + \lambda_2 b_{66}\sum_{m=1}^{M} C_{k_2m}^{(1)} u_{2k_1m} + \lambda_2 d_{66}\sum_{m=1}^{M} C_{k_2m}^{(1)} \psi_{x2k_1m} = 0, \\
&\kappa a_{66}\left(\eta_2 \psi_{x2Nk_2} + \sum_{n=1}^{N} C_{Nn}^{(1)} w_{2Nk_2}\right) = 0, \text{ at } \zeta_{2N}=1,
\end{aligned} \tag{48b}$$

$$\begin{aligned}
&a_{12}\sum_{n=1}^{N} C_{k_1n}^{(1)} u_{ink_2} + b_{12}\sum_{n=1}^{N} C_{k_1n}^{(1)} \psi_{xink_2} + \lambda_i a_{11}\sum_{m=1}^{M} C_{k_2m}^{(1)} v_{ik_1m} + \lambda_i b_{11}\sum_{m=1}^{M} C_{k_2m}^{(1)} \psi_{yik_1m} = 0, \\
&b_{12}\sum_{n=1}^{N} C_{k_1n}^{(1)} u_{ink_2} + d_{12}\sum_{n=1}^{N} C_{k_1n}^{(1)} \psi_{xink_2} + \lambda_i b_{11}\sum_{m=1}^{M} C_{k_2m}^{(1)} v_{ik_1m} + \lambda_i d_{11}\sum_{m=1}^{M} C_{k_2m}^{(1)} \psi_{yik_1m} = 0, \\
&a_{66}\sum_{n=1}^{N} C_{k_1n}^{(1)} v_{ink_2} + b_{66}\sum_{n=1}^{N} C_{k_1n}^{(1)} \psi_{xink_2} + \lambda_i a_{66}\sum_{m=1}^{M} C_{k_2m}^{(1)} u_{ik_1m} + \lambda_i b_{66}\sum_{m=1}^{M} C_{k_2m}^{(1)} \psi_{yik_1m} = 0, \\
&b_{66}\sum_{n=1}^{N} C_{k_1n}^{(1)} v_{ink_2} + d_{66}\sum_{n=1}^{N} C_{k_1n}^{(1)} \psi_{xink_2} + \lambda_i b_{66}\sum_{m=1}^{M} C_{k_2m}^{(1)} u_{ik_1m} + \lambda_i d_{66}\sum_{m=1}^{M} C_{k_2m}^{(1)} \psi_{yik_1m} = 0, \\
&\kappa a_{66}\left(\eta_i \psi_{yik_1k_2} + \lambda_i \sum_{m=1}^{M} C_{k_2m}^{(1)} w_{ik_1m}\right) = 0, \text{ at } \xi=0 \text{ and } \xi=1,
\end{aligned} \tag{48c}$$

for a CFFF plate. At $\zeta_1 = 1$, the following conditions should be satisfied

$$\begin{aligned}
&u_{1Nk_2} = u_{21k_2},\ v_{1Nk_2} = v_{21k_2},\ w_{1Nk_2} = w_{21k_2}, \\
&\psi_{x1Nk_2} = \psi_{x21k_2},\ \psi_{y1Nk_2} = \psi_{y21k_2},
\end{aligned} \tag{49a}$$

$$\begin{aligned}
&\frac{a_{11}}{\lambda_1}\sum_{n=1}^{N} C_{Nn}^{(1)} u_{1nk_2} + \frac{b_{11}}{\lambda_1}\sum_{n=1}^{N} C_{Nn}^{(1)} \psi_{x1nk_2} + a_{12}\sum_{m=1}^{M} C_{k_2m}^{(1)} v_{1Nm} + b_{12}\sum_{m=1}^{M} C_{k_2m}^{(1)} \psi_{y1Nm} \\
&= \frac{a_{11}}{\lambda_2}\sum_{n=1}^{N} C_{1n}^{(1)} u_{2nk_2} + \frac{b_{11}}{\lambda_2}\sum_{n=1}^{N} C_{1n}^{(1)} \psi_{x2nk_2} + a_{12}\sum_{m=1}^{M} C_{k_2m}^{(1)} v_{21m} + b_{12}\sum_{m=1}^{M} C_{k_2m}^{(1)} \psi_{y21m},
\end{aligned} \tag{49b}$$

$$\begin{aligned}
&\frac{b_{11}}{\lambda_1}\sum_{n=1}^{N} C_{Nn}^{(1)} u_{1nk_2} + \frac{d_{11}}{\lambda_1}\sum_{n=1}^{N} C_{Nn}^{(1)} \psi_{x1nk_2} + b_{12}\sum_{m=1}^{M} C_{k_2m}^{(1)} v_{1Nm} + d_{12}\sum_{m=1}^{M} C_{k_2m}^{(1)} \psi_{y1Nm} \\
&= \frac{b_{11}}{\lambda_2}\sum_{n=1}^{N} C_{1n}^{(1)} u_{2nk_2} + \frac{d_{11}}{\lambda_2}\sum_{n=1}^{N} C_{1n}^{(1)} \psi_{x2nk_2} + b_{12}\sum_{m=1}^{M} C_{k_2m}^{(1)} v_{21m} + d_{12}\sum_{m=1}^{M} C_{k_2m}^{(1)} \psi_{y21m},
\end{aligned} \tag{49c}$$

$$\begin{aligned}
&\frac{a_{66}}{\lambda_1}\sum_{n=1}^{N} C_{Nn}^{(1)} v_{1nk_2} + \frac{b_{66}}{\lambda_1}\sum_{n=1}^{N} C_{Nn}^{(1)} \psi_{y1nk_2} + a_{66}\sum_{m=1}^{M} C_{k_2m}^{(1)} u_{1Nm} + b_{66}\sum_{m=1}^{M} C_{k_2m}^{(1)} \psi_{x1Nm} \\
&= \frac{a_{66}}{\lambda_2}\sum_{n=1}^{N} C_{1n}^{(1)} v_{2nk_2} + \frac{b_{66}}{\lambda_2}\sum_{n=1}^{N} C_{1n}^{(1)} \psi_{y2nk_2} + a_{66}\sum_{m=1}^{M} C_{k_2m}^{(1)} u_{21m} + b_{66}\sum_{m=1}^{M} C_{k_2m}^{(1)} \psi_{x21m},
\end{aligned} \tag{49d}$$

$$\frac{b_{66}}{\lambda_1}\sum_{n=1}^{N}C_{Nn}^{(1)}v_{1nk_2}+\frac{d_{66}}{\lambda_1}\sum_{n=1}^{N}C_{Nn}^{(1)}\psi_{y1nk_2}+b_{66}\sum_{m=1}^{M}C_{k_2m}^{(1)}u_{1Nm}+d_{66}\sum_{m=1}^{M}C_{k_2m}^{(1)}\psi_{x1Nm}$$
$$=\frac{b_{66}}{\lambda_2}\sum_{n=1}^{N}C_{1n}^{(1)}v_{2nk_2}+\frac{d_{66}}{\lambda_2}\sum_{n=1}^{N}C_{1n}^{(1)}\psi_{y2nk_2}+b_{66}\sum_{m=1}^{M}C_{k_2m}^{(1)}u_{21m}+d_{66}\sum_{m=1}^{M}C_{k_2m}^{(1)}\psi_{x21m}, \tag{49e}$$

$$\eta_1\psi_{x1Nk_2}+\sum_{n=1}^{N}C_{Nn}^{(1)}w_{1nk_2}=\eta_2\psi_{x21k_2}+\sum_{n=1}^{N}C_{1n}^{(1)}u_{2nk_2}\ . \tag{49f}$$

The dimensionless form of unknown displacement vector **b** is

$$\mathbf{b}=\left\{\left\{u_{ik_{12}}\right\}^{\mathrm{T}},\left\{v_{ik_{12}}\right\}^{\mathrm{T}},\left\{w_{ik_{12}}\right\}^{\mathrm{T}},\left\{\psi_{xik_{12}}\right\}^{\mathrm{T}},\ \left\{\psi_{yik_{12}}\right\}^{\mathrm{T}}\right\}^{\mathrm{T}}, \tag{50}$$

where $i=\ 1,\ 2,\ k_{12}=M\times\left(k_1-\ 1\right)+k_2,\ k_1=\ 1,\ 2,\ \ldots,N,\ k_2=\ 1,\ 2,\ \ldots,M,k_{12}=\ 1,\ 2,\ \ldots,N\times M.$

The matrix expression of Eqs. (41)-(45) is,

$$\mathbf{Gb}+(\mathbf{M_f}+\mathbf{M})\ddot{\mathbf{b}}=\mathbf{0}, \tag{51}$$

where the added mass matrix $\mathbf{M}_\mathrm{f}$, the stiffness matrix **G** and the mass matrix **M** are all $10N\times10M$ matrices. The harmonic vibration are analyzed with the assumption of $\mathbf{b}=\mathbf{b}^*e^{i\omega\tau}$. Eq. (51) are rewritten as,

$$\left[\mathbf{G}-\omega^2(\mathbf{M_f}+\mathbf{M})\right]\mathbf{b}^*=\mathbf{0}\ . \tag{52}$$

For the fluid-plate interaction vibration problem, we need to solve the added mass matrix $\mathbf{M}_\mathrm{f}$ caused by the fluid pressure for FGM plates contacted with fluid. Herein, the added mass is dependent on the unknown vibrational mode shape $\mathbf{b}^*$ as shown in Eq. 10. Therefore, we use the iterative method to solve Eq. (52) by substituting the vibrational mode shape in vacuum as the initial value.

Applying the following iterative procedure, the natural frequency, and the mode shape of FGM rectangular plates partially immersed in a fluid are computed. The computational steps are:

(i) Solve ω and $\mathbf{b}^*$ for the vibration of FGM plates in vacuum from Eq. (52) with assuming $\mathbf{M_f}=\mathbf{0}$;

(ii) Apply the solution $\mathbf{b}^*$ obtained in step (i) to determine $\mathbf{M}_\mathrm{f}$, and the ω and $\mathbf{b}^*$ in Eq. (52) are calculated and updated;

(iii) Repeat step (ii) until the relative frequency error of two consecutive iterations is less than a prescribed tolerance, e.g., 10^{-5}.

3. Numerical results

Several numerical examples for the free vibration analysis of FGM plates that are partially immersed in a fluid are studied in this work. The fundamental frequency and mode shape of FGM plates in a fluid with respect to different

parameters, such as gradient index, the immersed depth, gradient type, aspect ratio, fluid density, and slenderness ratio are obtained and analyzed in this section. The material properties of SUS304 on the left surface of plates are E_a = 207.78 GPa, ρ_a = 8166 kg/m^3, υ_a = 0.3177, whereas those for Si_3N_4 on the right surface are E_b = 322.27 GPa, ρ_b = 2370 kg/m^3, υ_b = 0.24. Unless otherwise stated, FGM rectangular plates contact with water on both sides, and the plate parameters are: length L_x = 0.1 m, width L_y = 0.1 m, thickness h_0 = 0.01 m, and water density ρ_f = 1000 kg/m^3. The conversion $f = \Omega/2\pi$ is introduced for the computation of the fundamental frequency.

3.1 Model validation

The DQ method is used to solve the governing equations and obtain the fundamental frequency of FGM rectangular plates in a fluid. The convergence for the numerical procedure with respect to the use of different node numbers N, M, is testified and presented in Table 1. The numerical results for the fundamental frequency f of FGM plates in vacuum and that of half FGM plates immersed in water are obtained and listed in Table 1. For both two cases, the convergent results are achieved with the increase of N, and $M = N = 12$ is adopted in later computation and analysis.

Table 1 Convergence for the fundamental frequency f ($\times 10^3$ Hz) of FGM rectangular plates in vacuum and water (L_x = 0.1, L_y = 0.1, h_0 = 0.01, n = 1).

N	Plate in vacuum			Half of the plate immersed in water		
	C-C	H-H	C-F	C-C	H-H	C-F
4	24.829	14.013	0.98356	16.074	9.1985	0.91497
6	11.033	6.4207	1.1611	9.5818	5.5196	1.1477
8	10.992	6.4565	1.1634	9.5813	5.5347	1.1495
10	10.992	6.4559	1.1601	9.5767	5.5391	1.1473
12	10.992	6.4559	1.1587	9.5757	5.5395	1.1465
13	10.992	6.4559	1.1581	9.5753	5.5394	1.1465

The numerical results of frequency parameter $\omega^* = \Omega L_x^2 / h_0\sqrt{\rho_b / E_b}$ of SUS304/Si_3N_4 FGM rectangular plates in vacuum are obtained and presented in Table 2 for CCCC, SSSS and CFFF. The fundamental frequencies for CCCC, SSSS and CFFF FGM rectangular plates that were previously calculated by Zhao *et al.* [34] are used to verify the present results of FGM rectangular plates with different gradient variations. A good agreement between Zhao *et al.*'s

results and present solution is shown in Table 2.

Table 2 Dimensionless fundamental frequency $\omega^* = \Omega L_x / h_0 \sqrt{\rho_b / E_b}$ comparison for SUS304/ Si_3N_4 FGM plates in air ($L_x = L_y = 0.1$, $h_0 = 0.01$).

BCs		n					
		0	1	2	5	8	10
CCCC	present	9.7351	5.9228	5.3178	4.8301	4.6683	4.6051
	Zhao et al.[34]	9.6814	5.8902	5.2874	4.8005	4.6389	4.5767
SSSS	present	5.6809	3.4786	3.1321	2.8469	2.7498	2.7121
	Zhao et al. [34]	5.6148	3.4242	3.0813	2.8058	2.7129	2.6768
CFFF	present	1.0280	0.6251	0.5623	0.5121	0.4950	0.4884
	Zhao et al. [34]	1.0203	0.6199	0.5576	0.5077	0.4907	0.4841

Table 3 lists the results for fundamental frequency $\omega^* = \Omega L_y^2 \sqrt{\rho_{Al} t_{Al} / D}$ of CCCC, SSSS and CCCF aluminum plates contacted water with one side. The plate parameters are $L_x = L_y = 1$, $\mu = \rho_f / \rho_{Al} = 0.125$, $t_{Al} = h_0 = 0.05$, and $D = E_{Al} h_0^3 \Big/ \left[12(1 - v_{Al}^2)\right]$. The material properties of aluminum plates are $E_{Al} = 30$ GPa, $\rho_{Al} = 8000$ kg/m^3, $\upsilon_{Al} = 0.3$. Zhou and Cheung [46] analyzed the variations of fundamental frequency of vertical rectangular Kirchhoff plates with respect to the increase of immersed depth using the Ritz method. The results of Zhou and Cheung [46] are used to verify the results obtained using present method.

Table 3 Dimensionless fundamental frequency for rectangular FGM plates contacted with water on one side ($n = 0$, $L_x = L_y = 1$, $h_0 = 0.05$).

BCs		g_1			
		0	0.2	0.4	0.6
CCCC	present	34.985	34.941	33.723	29.747
	Zhou and Cheung [46]	36.007	35.968	34.216	31.273
SSSS	present	19.562	19.488	18.587	16.460
	Zhou and Cheung [46]	19.739	19.666	18.451	16.854
CCCF	present	23.425	23.423	23.320	22.571
	Zhou and Cheung [46]	24.035	24.033	23.873	23.294

3.2 Effect of different parameters on fundamental frequency

Fig. 2 shows the variation trends for the fundamental frequency with respect to the gradient index n for the CCCC, SSSS and CFFF FGM rectangular plates partially immersed in water when $L_x/L_y = 1$ and $L_x/h_0 = 10$. The frequency reduces with the increase of the immersed depth g_1 for all three plates. Besides, an obvious decrease of fundamental frequency occurs at $g_1 \in [0.2, 1]$ for CCCC and SSSS plates, and $g_1 \in [0.5, 1]$ for CFFF plates. For immersed depth g_1 with a given value, the fundamental frequency decreases remarkably as the gradient index n increases for all three plates.

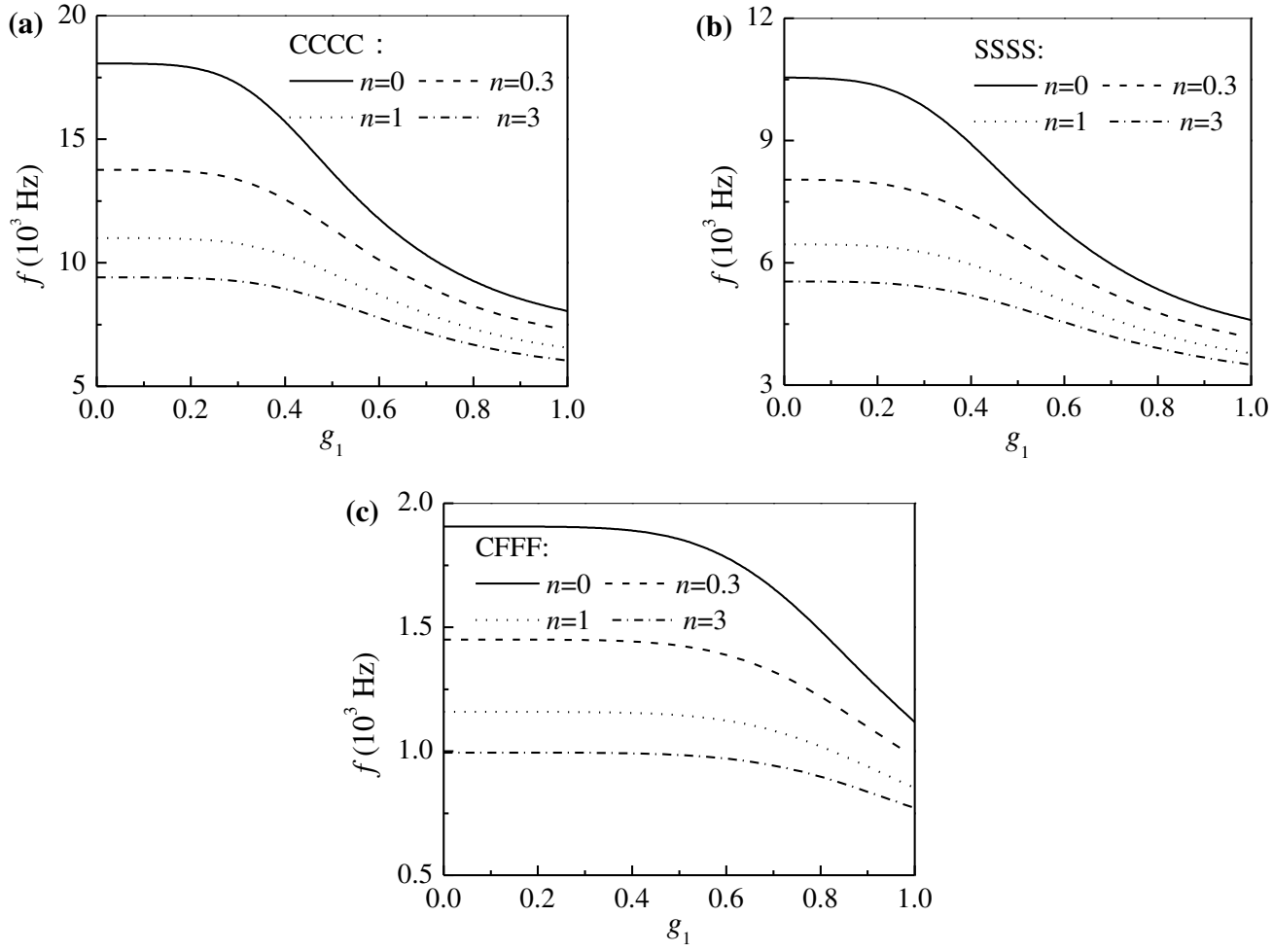

Fig. 2. The response of the fundamental frequency on the gradient index n for FGM rectangular plates in water when with $L_x/L_y = 1$ and $L_x/h_0 = 10$: (a) CCCC plate; (b) SSSS plate and (c) CFFF plate.

The change of fundamental frequency with different fluid media for CCCC, SSSS and CFFF FGM rectangular plates is illustrated in Fig. 3 when $L_x/L_y = 1$, $n = 1$ and $L_x/h_0 = 10$. Herein, the numerical results with different fluid media of bromoform (2.82 g/cm^3), water (1 g/cm^3) and acetone (0.788 g/cm^3) are obtained and discussed. The different fluid media have a neglected influence at the immersed depth $g_1 \in [0, 0.1]$ for CCCC and SSSS plates, and $g_1 \in [0, 0.3]$ for CFFF plates. Smaller fluid density ρ_f lead to larger fundamental frequency when $g_1 \in [0.3, 1]$.

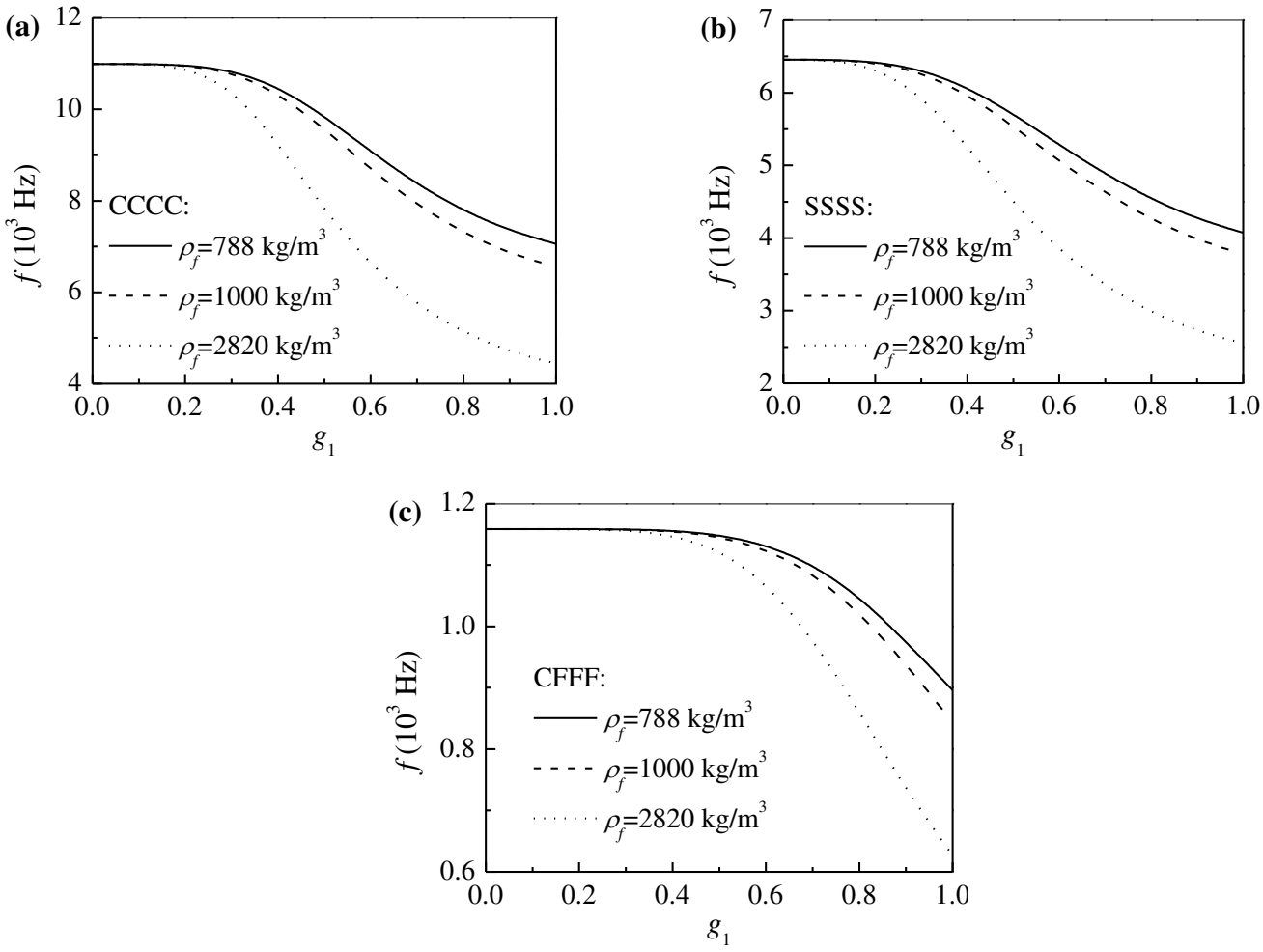

Fig. 3. The change of the fundamental frequency on the fluid media for FGM plates in water when L_x/L_y = 1, n = 1 and L_x/h_0 = 10: (a) CCCC plate; (b) SSSS plate and (c) CFFF plate.

Fig. 4 depicted the change of fundamental frequency with different aspect ratios L_x/L_y for CCCC, SSSS and CFFF FGM rectangular plates in water when n = 1 and L_x/h_0 = 10. As shown in Fig. 4-(a) and (b), the fundamental frequency is quite sensitive to the aspect ratio and increases with the increasing of the aspect ratio of CCCC and SSSS plates. However, the change of fundamental frequency with different aspect ratios for CFFF FGM plates is very small. With the same parameters, CCCC and CFFF submerged plates have the largest and smallest fundamental frequency, respectively.

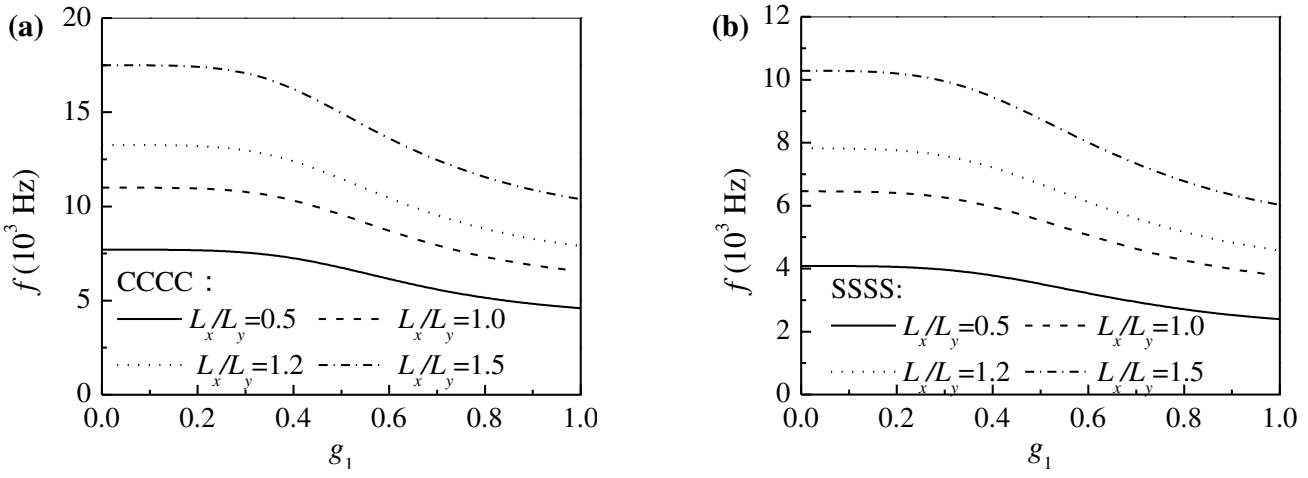

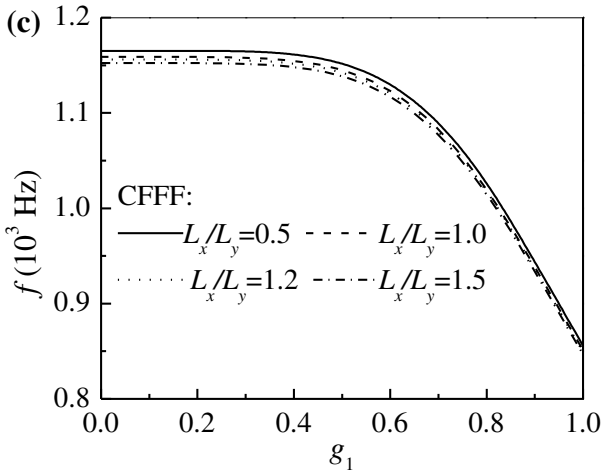

Fig. 4. The change of the fundamental frequency on the aspect ratio L_x/L_y for FGM plates in water when n = 1 and L_x/h_0 = 10: (a) CCCC plate; (b) SSSS plate and (c) CFFF plate.

Fig. 5 illustrates the effect of changing the slenderness ratio L_x/h_0 on the fundamental frequency for CCCC, SSSS and CFFF FGM rectangular plates immersed in water when L_x/L_y = 1 and n = 1. For any given g_1, the larger slenderness ratio L_x/h_0 leads to the smaller fundamental frequency for all three FGM plates.

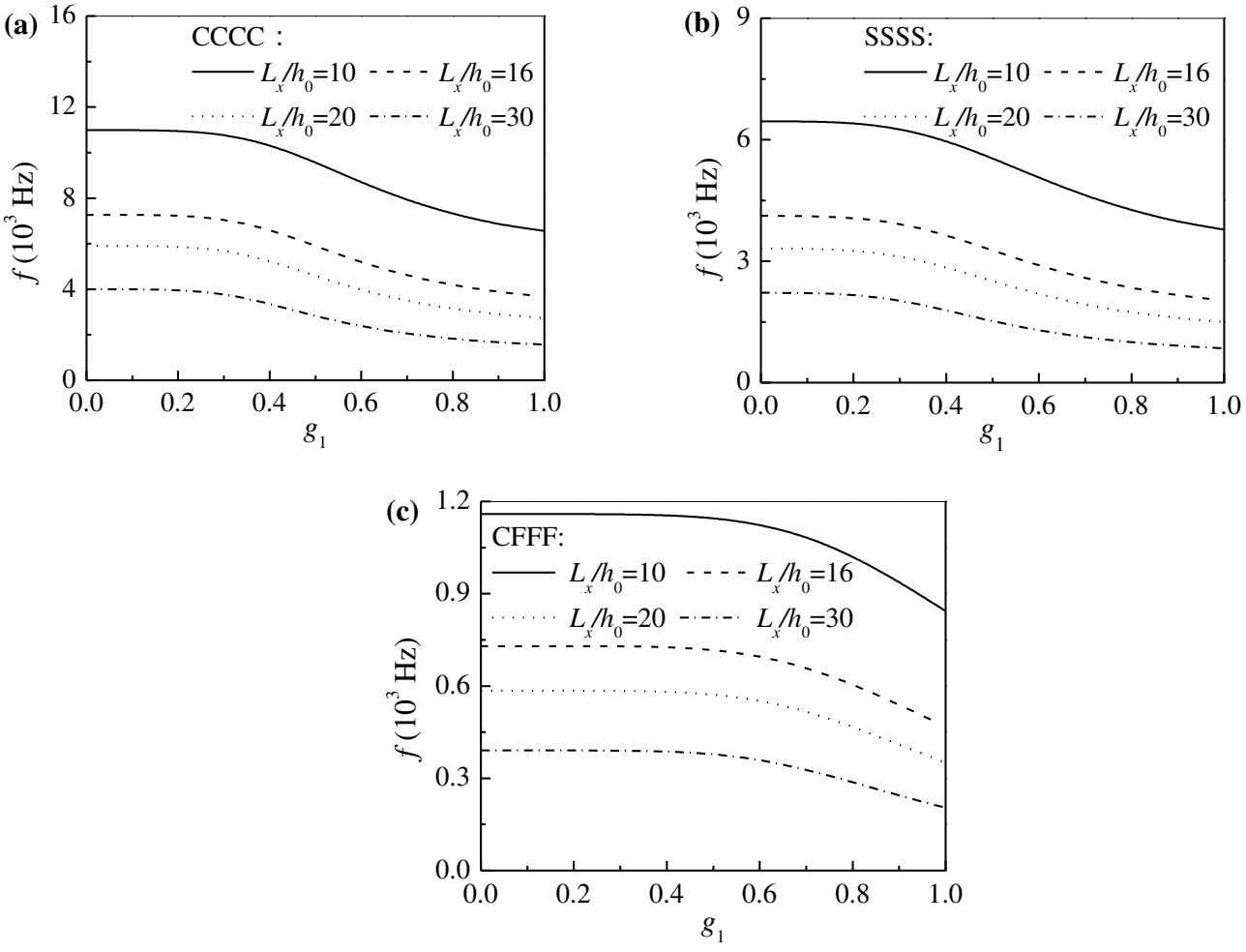

Fig. 5. The effect of the slenderness ratio L_x/h_0 on the fundamental frequency for FGM plates in water when L_x/L_y = 1 and n = 1: (a) CCCC plate; (b) SSSS plate and (c) CFFF plate.

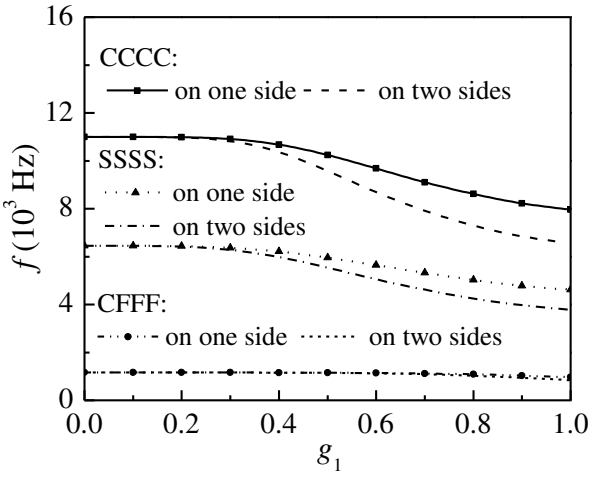

Fig. 6. The fundamental frequency of the FGM plates contacted with water on one sides and two sides when $L_x/L_y = 1$, $n = 1$ and $L_x/h_0 = 10$.

Fig. 6 presents the fundamental frequencies of CCCC, SSSS and CFFF FGM rectangular plates contacted with water on one side when $L_x/L_y = 1$, $n = 1$ and $L_x/h_0 = 10$. The results for the plates contacting with water on two sides are also given for the comparison purpose. For both CCCC and SSSS FGM plates, the difference of fundamental frequency is unobvious when $g_1 \in [0, 0.2]$. However, in general, the fundamental frequency of FGM plates contacted with water on one side is larger than that of two sides. Larger difference between these two cases will occur when the immersed depth g_1 is increasing from 0.2 to 1.0. For CFFF FGM plates, the fundamental frequencies for these two cases are almost identical.

Fig. 7 shows the change of the fundamental mode shape on the immersed depth g_1 for CCCC, SSSS and CFFF FGM plates in water when $L_x/L_y = 1$, $n = 1$, $L_x/h_0 = 10$, and $\xi = 0.5$. The fundamental mode shape in air is symmetrical for CCCC and SSSS FGM plates. However, for CCCC and SSSS FGM plates, the mode shape in fluid deviates from that in air and shows an unsymmetrical shape. For CFFF FGM plates, the change of the mode shape on the immersed depth is unobvious.

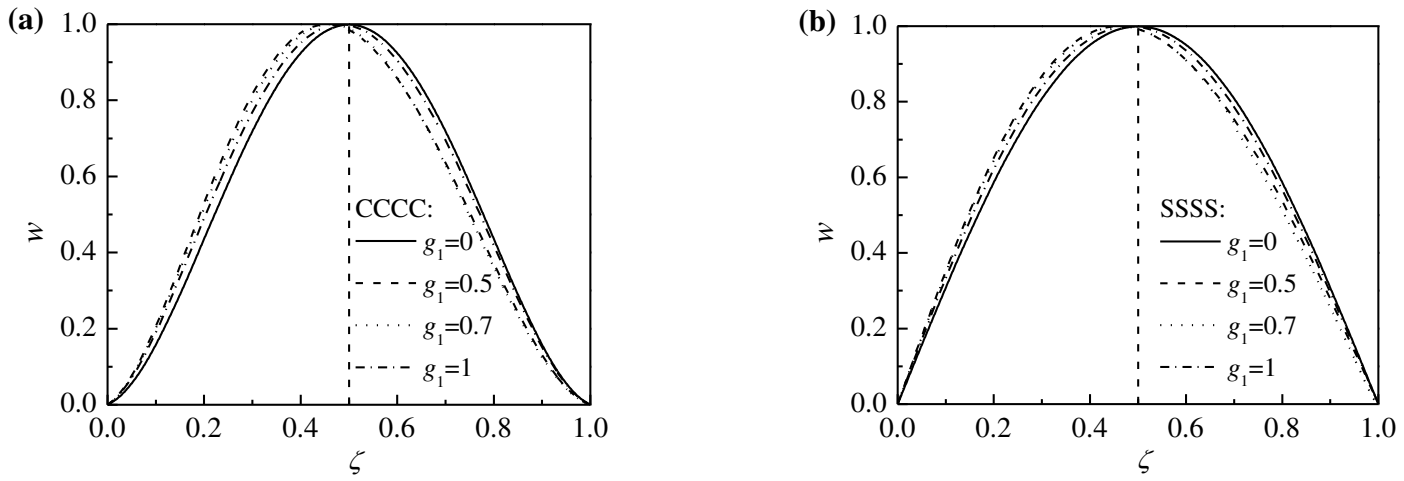

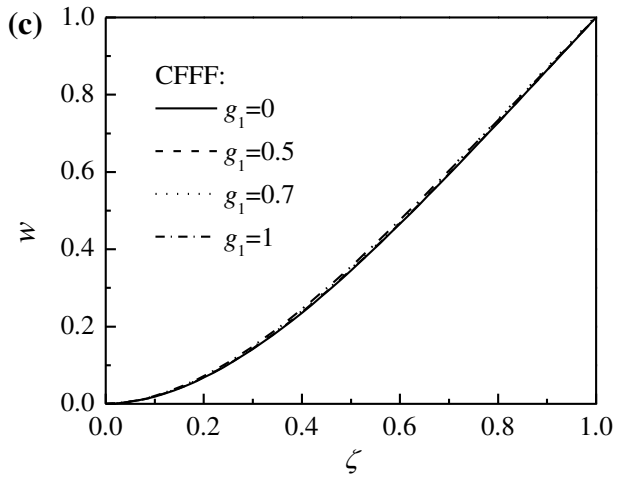

Fig. 7. The change of the mode shape on the immersed depth g_1 for FGM plates in water when $L_x/L_y = 1$, $n = 1$, $L_x/h_0 = 10$ and $\xi = 0.5$: (a) CCCC plate; (b) SSSS plate; (c) CFFF plate.

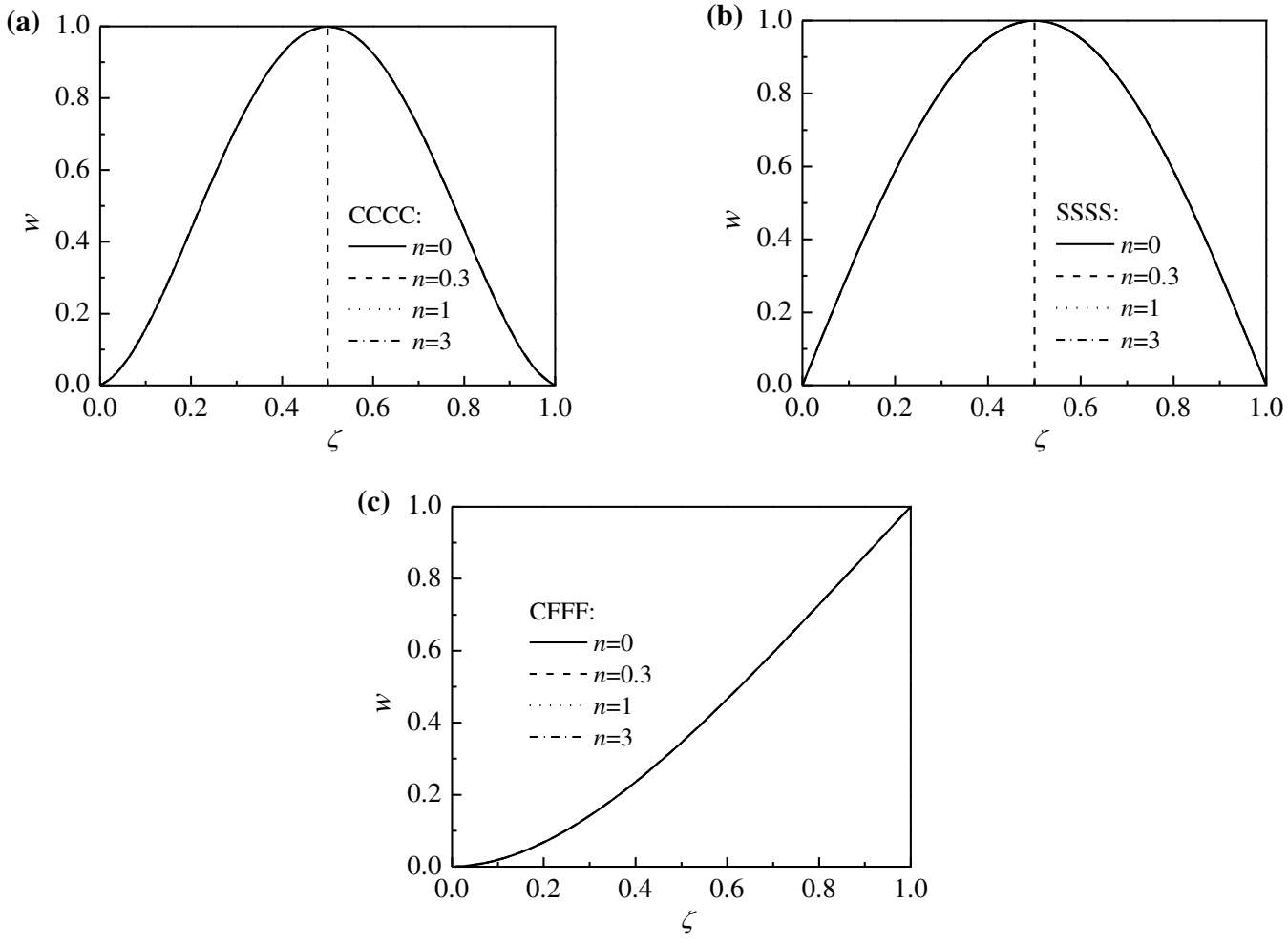

Fig. 8. The response of the mode shape on the gradient index n for FGM plates in air when $L_x/L_y = 1$, $g_1 = 0$, $L_x/h_0 = 10$ and $\xi = 0.5$: (a) CCCC plate; (b) SSSS plate; (c) CFFF plate.

Figs. 8-10 present the response of the fundamental mode shape of CCCC, SSSS and CFFF FGM plates with different gradient index n when $L_x/L_y = 1$, $L_x/h_0 = 10$, and $\xi = 0.5$ for $g_1 = 0$, $g_1 = 0.5$ and $g_1 = 1$, respectively. As shown

in Figs. 8 and 9, the change of the fundamental mode shape with respect to different gradient index n is insignificant for all three FGM plates either in air or in water. Fig. 10 indicates that with the decrease of gradient index n, the deviation of mode shape increases for CCCC and SSSS FGM rectangular plates in fluid with $g_1 = 0.5$. However, the change of the mode shape on gradient index n is very sight for CFFF rectangular plates. The effect of other parameters is unobvious on the fundamental mode shape.

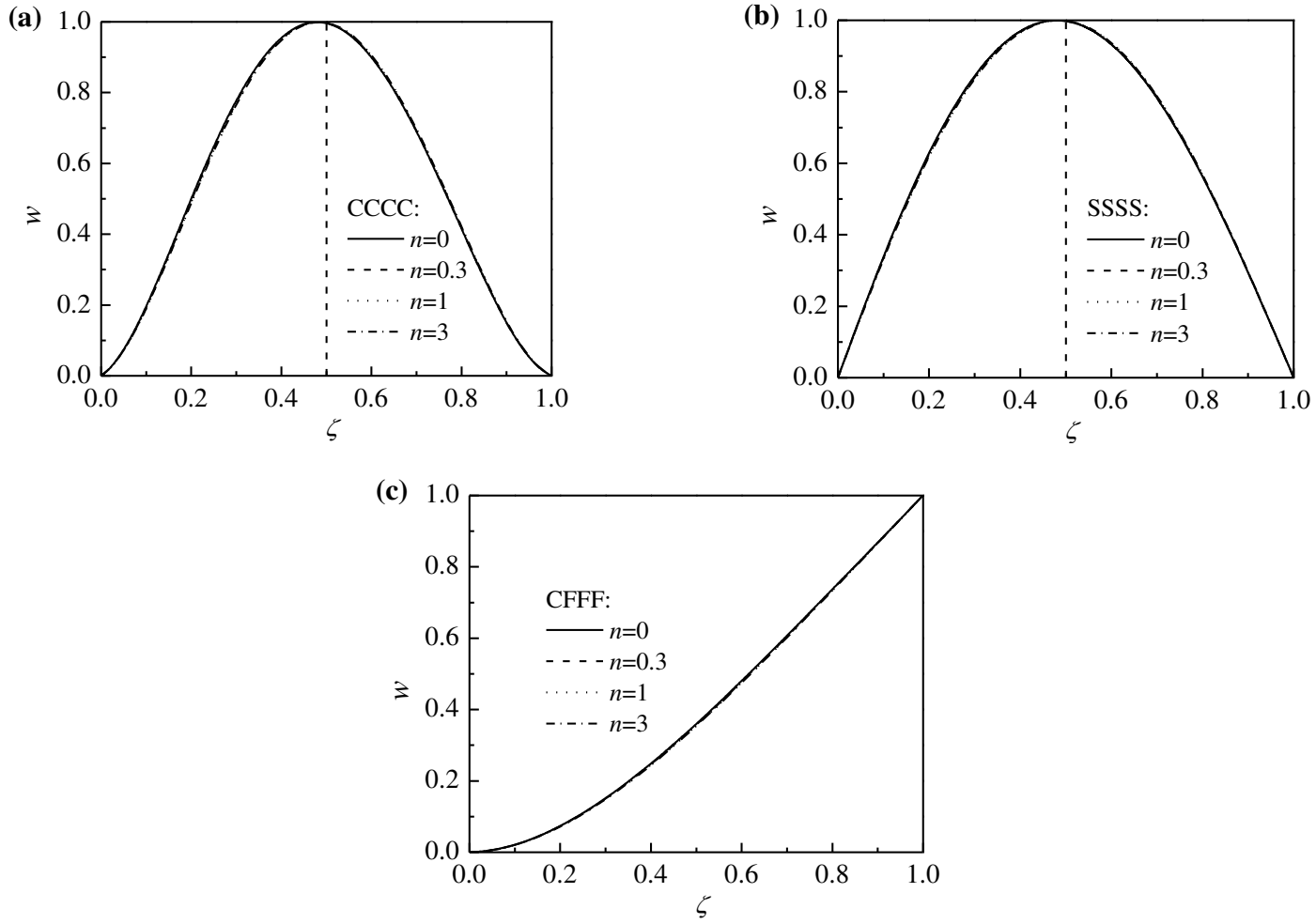

Fig. 9. The response of the mode shape on the gradient index n for FGM plates in water when $L_x/L_y = 1$, $g_1 = 1$, $L_x/h_0 = 10$ and $\xi = 0.5$: (a) CCCC plate; (b) SSSS plate; (c) CFFF plate.

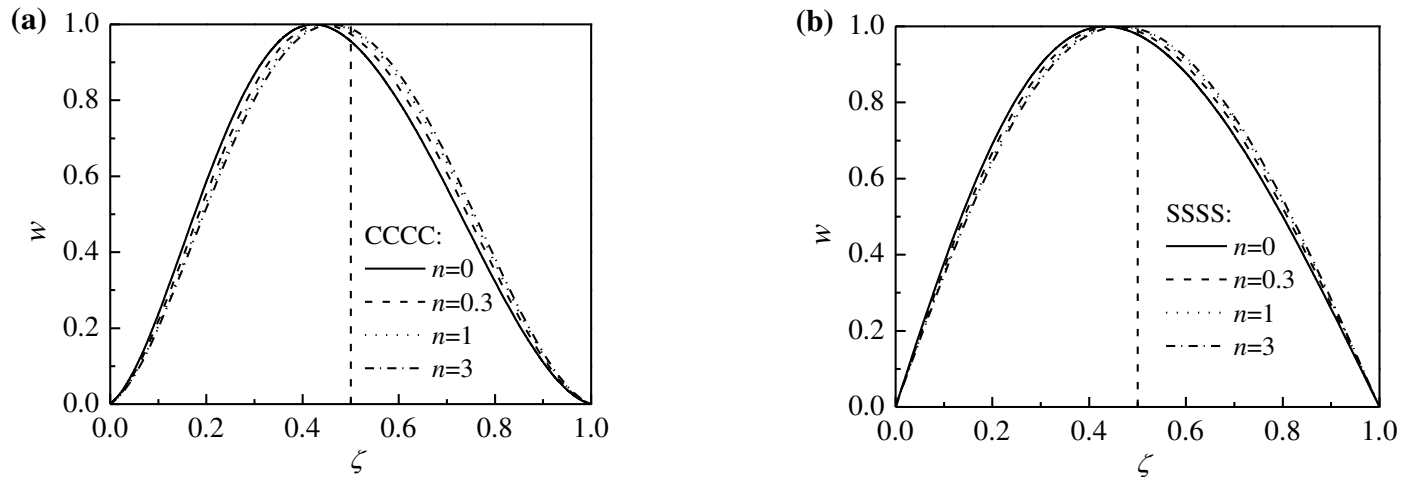

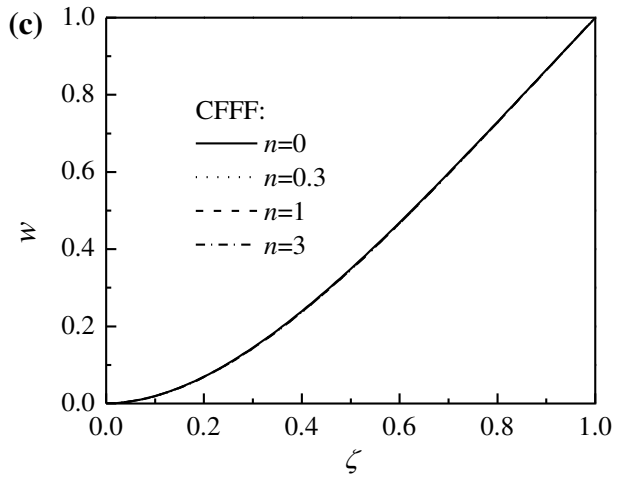

Fig. 10. The response of the mode shape on the gradient index n for FGM plates in water when $L_x/L_y = 1$, $g_1 = 0.5$, $L_x/h_0 = 10$ and $\xi = 0.5$: (a) CCCC plate; (b) SSSS plate; (c) CFFF plate.

3.3 Change of fundamental frequency and mode shape on gradient type

The change of fundamental frequency of FGM plates with different material gradient types in contacting with water is analyzed in this sub-section. Four gradient types including the power law, sinusoidal, cosine and exponential forms, are proposed to describe the distribution of material properties. The change of the Young's modulus versus thickness z/h_0 for different gradient types is given in Fig. 11. For different gradient types, the materials of FGM plate are assumed as SUS304 and Si_3N_4 at $z/h_0 = -0.5$ and $z/h_0 = 0.5$, respectively. The Young's modulus for four gradient types are continuously varied form $z/h_0 = -0.5$ to $z/h_0 = 0.5$. The expressions of different gradient types are listed below [46]:

(a) Power law form is given in Eqs. (1)-(3) and $n = 3$ is used for comparison with other gradient types;

(b) Exponential form for the variation of material parameters is formulated as:

$$E(z) = E_a e^{\beta_1 (z/h_0 + 0.5)},\ \beta_1 = \ln(E_b / E_a), \tag{53a}$$

$$\rho(z) = \rho_a e^{\beta_2 (z/h_0 + 0.5)},\ \beta_2 = \ln(\rho_b / \rho_a), \tag{53b}$$

$$v(z) = v_a e^{\beta_3 (z/h_0 + 0.5)},\ \beta_3 = \ln(v_b / v_a), \tag{53c}$$

(c) Sinusoidal form is formulated as:

$$E(z) = (E_b - E_a) \sin\left(\frac{\pi (z/h_0 + 0.5)}{2} \right) + E_a, \tag{54a}$$

$$\rho(z) = (\rho_b - \rho_a) \sin\left(\frac{\pi (z/h_0 + 0.5)}{2} \right) + \rho_a, \tag{54b}$$

$$v(z) = (v_b - v_a)\sin\left(\frac{\pi(z/h_0+0.5)}{2}\right) + v_a, \tag{54c}$$

(d) Cosine form is formulated as:

$$E(z) = \frac{(E_b + E_a)}{2} - \frac{(E_b - E_a)}{2}\cos\left(\pi(z/h_0+0.5)\right), \tag{55a}$$

$$\rho(z) = \frac{(\rho_b + \rho_a)}{2} - \frac{(\rho_b - \rho_a)}{2}\cos\left(\pi(z/h_0+0.5)\right), \tag{55b}$$

$$v(z) = \frac{(v_b + v_a)}{2} - \frac{(v_b - v_a)}{2}\cos\left(\pi(z/h_0+0.5)\right). \tag{55c}$$

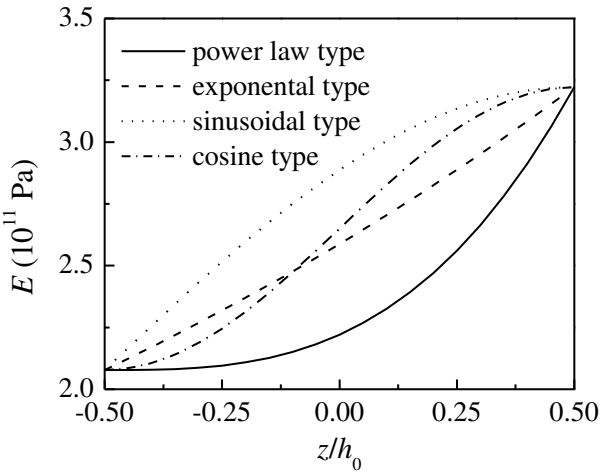

Fig. 11. The change of Young's modulus versus thickness z/h_0 for different gradient types.

The change of fundamental frequency with respect to different material gradient types for FGM plates in water when $L_x/L_y = 1$ and $L_x/h_0 = 10$ is illustrated in Fig. 12. Among four different gradient types, the power law type has the smallest fundamental frequency, and the sinusoidal form has the largest fundamental frequency. For the four different gradient types, the difference of fundamental frequency decreases with increasing of the immersed depth g_1.

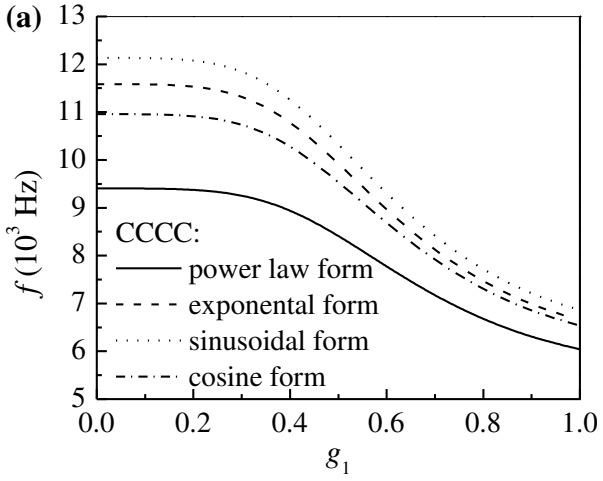

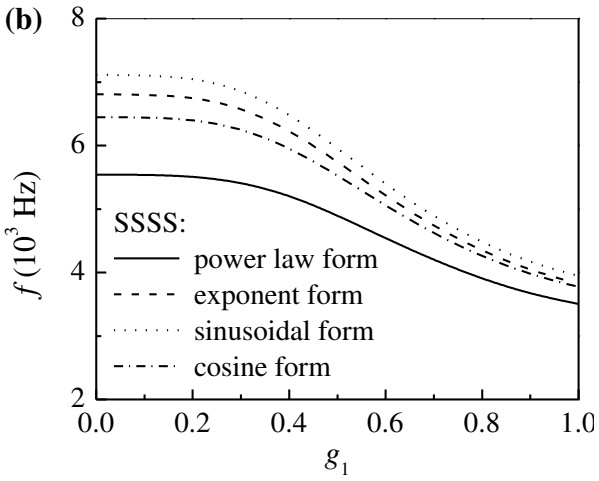

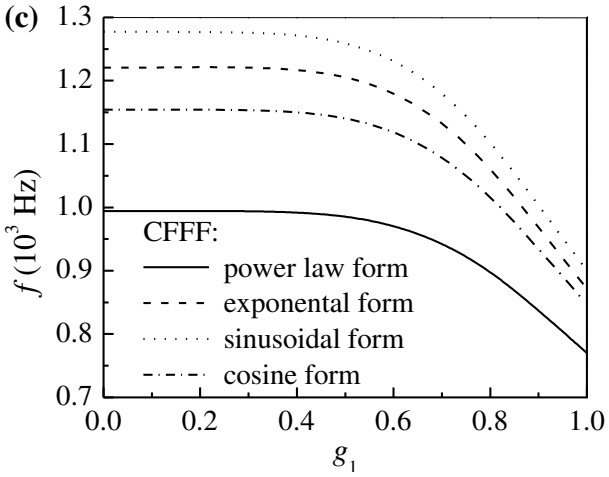

Fig. 12. The change of the fundamental frequency on different gradient types for FGM plates in water when L_x/L_y = 1 and L_x/h_0 = 10: (a) CCCC plate; (b) SSSS plate and (c) CFFF plate.

Fig. 13 shows the change of the mode shape on different material gradient types for CCCC, SSSS and CFFF FGM rectangular plates in water when L_x/L_y = 1, g_1 = 0.5 and L_x/h_0 = 10. The mode shape is not sensitive to the different gradient types for all three FGM rectangular plates.

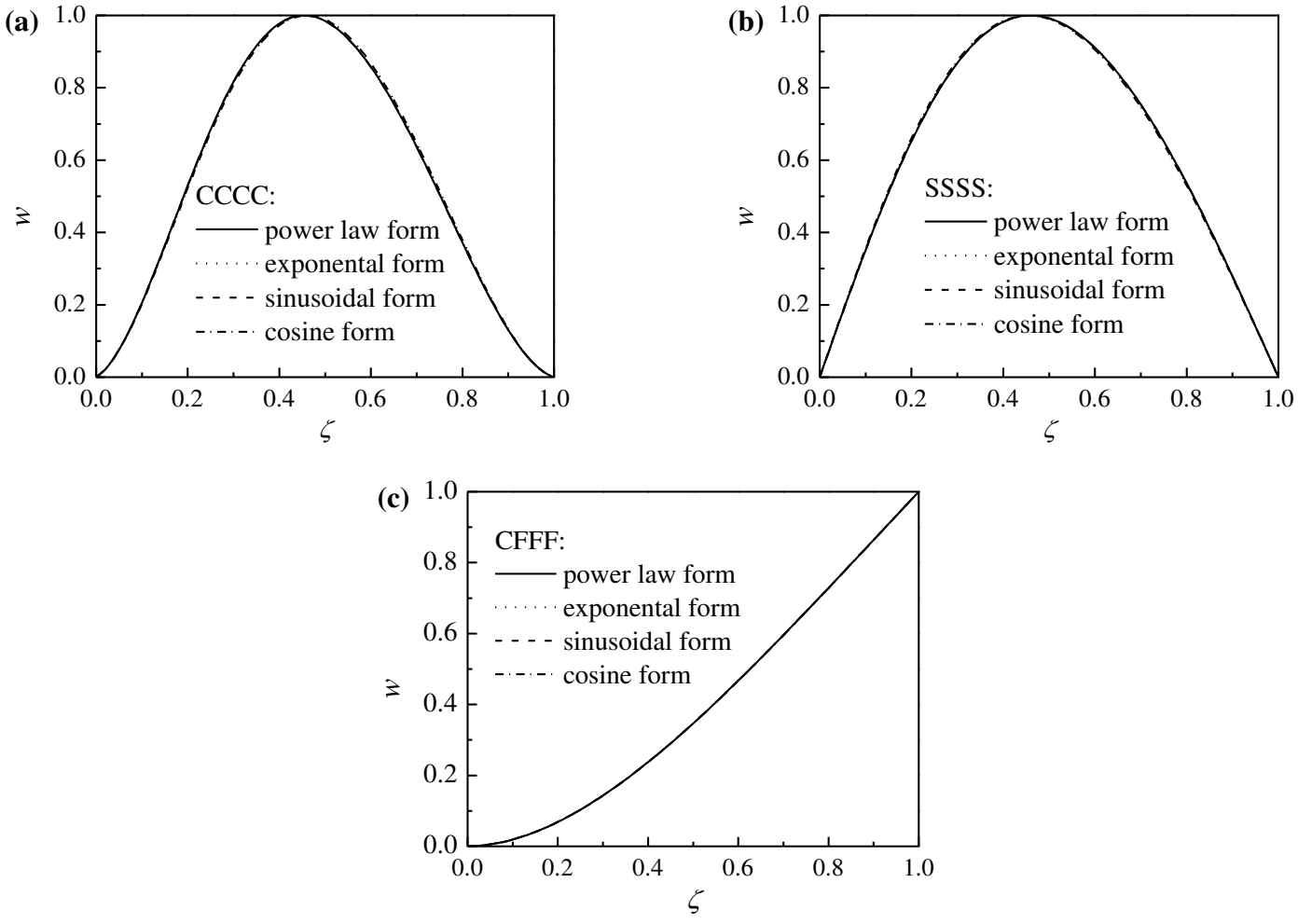

Fig. 13. The change of the mode shape on different gradient types for FGM plates in water when L_x/L_y = 1, g_1 = 0.5, L_x/h_0 = 10 and ξ = 0.5: (a) CCCC plate; (b) SSSS plate and (c) CFFF plate.

4. Conclusions

This paper focus on the study of free vibration of FGM Mindlin plates with rectangular cross-section contacted with an incompressible and inviscid fluid. The fluid loading is considered as an added mass to the vibration of plates. The governing equations and the boundary conditions are derived with discretized forms by the DQ method and the variational principle. Based on the discretized governing equations, the fundamental frequency and modal of plate-fluid coupling system are calculated using an iterative procedure. Numerical examples are performed to show the change of vibration characteristic on key parameters, such as gradient index, immersed depth, gradient type, fluid density, aspect ratio and slenderness ratio. Several important conclusive points are summarized as,

(1) The fundamental frequency decreases with the increase of the material gradient index for all three FGM plates.

(2) The larger fluid density and slenderness ratio lead to the smaller fundamental frequency for all three plates.

(3) The fundamental frequency increases for CCCC and SSSS plates in fluid when the aspect ratio of the plates is increasing.

(4) The fundamental frequency difference between the cases of one side and two sides contacting with fluid is increasing when the immersed depth is increased.

(5) Among four different material gradient types, the FGM plate with power law type gradient has the smallest fundamental frequency, while the one with sinusoidal form has the largest value.

(6) For CCCC and SSSS FGM plates, the mode shape in fluid deviates from that in vacuum, and show unsymmetrical mode shapes.

Acknowledgements

The authors thankfully appreciate the supports from the Fundamental Research Funds for the Central Universities (No. 2020YJS111), and the National Natural Science Foundation of China (Nos. 11725207, 12021002 and 12072226).

References

[1] Zamanzadeh M, Rezazadeh G, Jafarsadeghi-Poornaki I, Shabani R. Static and dynamic stability modeling of a capacitive FGM micro-beam in presence of temperature changes. Appl Math Model 2013;37:6964–6978.

[2] Wattanasakulpong N, Bui TQ. Vibration analysis of third-order shear deformable FGM beams with elastic support by Chebyshev collocation method. Int J Struct Stab Dyn 2018;18(5):1850071.

[3] Yang J, Kitipornchai S, Liew KM. Non-linear analysis of the thermo-electro-mechanical behaviour of shear deformable FGM plates with piezoelectric actuators. Int J Numer Meth Eng 2004;59(12):1605–1632.

[4] Shen HS, Xiang Y, Lin F. Nonlinear vibration of functionally graded graphene-reinforced composite laminated plates in thermal environments. Comput Method Appl M 2017; 319: 175-193.

[5] Sofiyev AH. The vibration and stability behavior of freely supported FGM conical shells subjected to external pressure. Compos Struct 2009;89(3):356–366.

[6] Lu L, Guo XM, Zhao JZ. On the mechanics of Kirchhoff and Mindlin plates incorporating surface energy. Int J Eng Sci 2018;124:24–40.

[7] Wang CM, Lee KH. Buckling load relationship between Reddy and Kirchhoff circular plates. J Franklin I 1998;335(6):989–995.

[8] Wang CM, Kitipornchai S, Xiang Y. Relationships between buckling loads of Kirchhoff, Mindlin, and Reddy polygonal plates on Pasternak foundation. J Eng Mech 1997;123(11):1134–1137.

[9] Mora D, Rivera G, Velásquez I. A virtual element method for the vibration problem of Kirchhoff plates. ESAIM Math Model Numer Anal 2018;52(4):1437–1456.

[10] Minh PP, Duc ND. The effect of cracks on the stability of the functionally graded plates with variable-thickness using HSDT and phase-field theory. Compos B Eng 2019;175:107086.

[11] Selim BA, Zhang LW, Liew KM. Active vibration control of FGM plates with piezoelectric layers based on Reddy's higher-order shear deformation theory. Compos Struct 2016;155:118–134.

[12] Roque CMC, Ferreira AJM, Reddy JN. Analysis of Mindlin micro plates with a modified couple stress theory and a meshless method. Appl Math Model 2013;37(7):4626–4633.

[13] Fares ME, Elmarghany MK, Atta D. An efficient and simple refined theory for bending and vibration of functionally graded plates. Compos Struct 2009;91(3):296–305.

[14] Yang J, Huang XH, Shen HS. Nonlinear flexural behavior of temperature-dependent FG-CNTRC laminated beams with negative Poisson's ratio resting on the Pasternak foundation. Eng Struct 2020;207:110250.

[15] Eftekhari SA, Jafari AA. Modified mixed Ritz-DQ formulation for free vibration of thick rectangular and skew plates with general boundary conditions. Appl Math Model 2013;37:7398–7426.

[16] Baferani AH, Saidi AR, Ehteshami H. Accurate solution for free vibration analysis of functionally graded thick rectangular plates resting on elastic foundation. Compos Struct 2011;93(7):1842–1853.

[17] Demirhan PA, Taskin V. Bending and free vibration analysis of Levy-type porous functionally graded plate using state space approach. Compos B Eng 2019;160:661–676.

[18] Shen HS, Xiang Y. Nonlinear analysis of nanotube-reinforced composite beams resting on elastic foundations in t hermal environments. Eng Struct 2013;56(6):698–708.

[19] Narendar S. Buckling analysis of micro-/nano-scale plates based on two-variable refined plate theory incorporating nonlocal scale effects. Compos Struct 2011;93(12):3093–3103.

[20] Jalali SK, Naei MH, Poorsolhjouy A. Buckling of circular sandwich plates of variable core thickness and FGM face sheets. Int J Struct Stab Dyn 2011;11(02):273–295.

[21] Shen HS, Lin F, Xiang Y. Nonlinear bending and thermal postbuckling of functionally graded graphene-reinforced composite laminated beams resting on elastic foundations. Eng Struct 2017;140:89–97.

[22] Shen HS. Nonlinear analysis of simply supported Resissner-Mindlin plates subjected to lateral pressure and thermal loading and resting on two-parameter elastic foundations. Eng Struct 2000;22(11):1481–1493.

[23] Wu LH, Wang HJ, Wang DB. Dynamic stability analysis of FGM plates by the moving least squares differential quadrature method. Compos Struct 2007;77(3):383–394.

[24] Yang J, Liew KM, Kitipornchai S. Dynamic stability of laminated FGM plates based on higher-order shear deformation theory. Comput Mech 2004;33(4):305–315.

[25] Hosseini-Hashemi S, Taher HRD, Akhavan H, Omidi M. Free vibration of functionally graded rectangular plates using first-order shear deformation plate theory. Appl Math Model 2010;34(5):1276–1291.

[26] Beni AA. Free vibration of functionally graded arbitrary straight-sided quadrilateral plates resting on elastic foundations. Int J Appl Mech 2011;3(04):825–843.

[27] Roshan L, Neha A. Buckling and Vibration of Functionally Graded Non-uniform Circular Plates Resting on Winkler Foundation. Latin Amer J Solids Struct 2015;12(12):2231–2258.

[28] Hosseini-Hashemi S, Fadaee M, Atashipour SR. Study on the free vibration of thick functionally graded rectangular plates according to a new exact closed-form procedure. Compos Struct 2011;93(2):722–735.

[29] Thai HT, Park T, Choi DH. An efficient shear deformation theory for vibration of functionally graded plates. Arch Appl Mech 2013;83(1):137–149.

[30] Talha M, Singh BN. Static response and free vibration analysis of FGM plates using higher order shear deformation theory. Appl Math Model 2010;34(12):3991–4011.

[31] Hosseini-Hashemi S, Fadaee M, Atashipour SR. A new exact analytical approach for free vibration of Reissner–Mindlin functionally graded rectangular plates. Int J Mech Sci 2011;53(1):11–22.

[32] Kim K, Kim K, Han C, Jang Y, Han P. A method for natural frequency calculation of the functionally graded rectangular plate with general elastic restraints. AIP Adv 2020;10(8):085203.

[33] Wang ZX, Shen HS. Nonlinear vibration of nanotube-reinforced composite plates in thermal environments. Comput Mater Sci 2011;50(8):2319–2330.

[34] Zhao X, Lee YY, Liew KM. Free vibration analysis of functionally graded plates using the element-free kp-Ritz method. Comput Method Appl Mech Eng 2009;319(3-5):918–939.

[35] Farsani SR, Jafari-Talookolaei RA, Valvo PS, Goudarzi AM. Free vibration analysis of functionally graded porous plates in contact with bounded fluid. Ocean Eng 2020;219:108285.

[36] Thinh TI, Tu TM, Long NV. Free vibration of a horizontal functionally graded rectangular plate submerged in fluid medium. Ocean Eng 2020;216:107593.

[37] Wu ZM, Ma XH, Brett PN, Xu JW. Vibration analysis of submerged rectangular microplates with distributed mass loading. Proc Roy Soc A-Math Physical and Eng Sci 2009;465:1323–1336.

[38] Wu ZM, Wright MT, Ma XH. The experimental evaluation of the dynamics of fluid-loaded microplates. J Micromech Microeng 2010;20(7):075034.

[39] Canales FG, Mantari JL. Discrepancy on the free vibration of laminated composite plates coupled to a compressible and incompressible fluid domain. Ocean Eng 2018;167:267–281.

[40] Liao CY, Ma CC. Vibration characteristics of rectangular plate in compressible inviscid fluid. J Sound Vib 2016;362:228–251.

[41] Akbarov SD, Ismailov MI. Frequency response of a viscoelastic plate under compressible viscous fluid loading. Appl Comput Math 2014;8(1):332–344.

[42] Khorshidi K, Karimi M. Analytical modeling for vibrating piezoelectric nanoplates in interaction with inviscid fluid using various modified plate theories. Ocean Eng 2019;181:267–280.

[43] Kozlovsky Y. Vibration of plates in contact with viscous fluid: Extension of Lamb's model. J Sound Vib 2009;326(1-2):332–339.

[44] Hosseini-Hashemi S, Arpanahi RA, Rahmanian S, Ahmadi-Savadkoohi A. Free vibration analysis of nano-plate in viscous fluid medium using nonlocal elasticity. Eur J Mech A-Solid 2019;74:440–448.

[45] Canales FG, Mantari JL. Vibrational behavior of isotropic plate structures in contact with a bounded fluid via unified formulation. Chinese J Aeronaut 2019;32(04):155–171.

[46] Zhou D, Cheung YK. Vibration of vertical rectangular plate in contact with water on one side. Earthq Eng Struct Dyn 2015;29(5):693–710.

[47] Omiddezyani S, Jafari-Talookolaei RA, Abedi M, Afrasiab H. The size-dependent free vibration analysis of a rectangular Mindlin microplate coupled with fluid. Ocean Eng 2018;163:617–629.

[48] Khorshidi K, Akbari F, Ghadirian H. Experimental and analytical modal studies of vibrating rectangular plates in contact with a bounded fluid. Ocean Eng 2017;140:146–154.

[49] Bochkarev SA, Kamenskikh AO, Lekomtsev SV. Experimental investigation of natural and harmonic vibrations of plates interacting with air and fluid. Ocean Eng 2020;206:107341.

[50] Liu J, Ke LL, Wang YS, Yang J, Alam F. Thermoelastic frictional contact of functionally graded materials with arbitrarily varying properties. Int J Mech Sci 2012;63(1):86–98.

[51] Hosseini-Hashemi S, Karimi M, Rokni H. Natural frequencies of rectangular Mindlin plates coupled with stationary fluid. Appl Math Model 2012;36(2):764–778.

[52] Li J, Guo XH, Luo J, Li HY, Wang YQ. Analytical study on inherent properties of a unidirectional vibrating steel strip partially immersed in fluid. Shock Vib 2013;20(4):793–807.

[53] Efraim E, Eisenberger M. Exact vibration analysis of variable thickness thick annular isotropic and FGM plates. J Sound Vib 2007; 299:720–738.

[54] Shu C. Differential quadrature and its application in engineering. Springer London; 2000.